THE UNIVERSITY OF ALBERTA

[illegible] OF SOME DEUTERON STRIPPING REACTIONS

by

GARY DALE WAIT

A THESIS
SUBMITTED TO THE FACULTY OF GRADUATE STUDIES
IN PARTIAL FULFILMENT OF THE REQUIREMENTS FOR THE DEGREE
OF MASTER OF SCIENCE

DEPARTMENT OF PHYSICS
EDMONTON, ALBERTA

September, 1964

THE UNIVERSITY OF ALBERTA

STUDIES OF SOME DEUTERON STRIPPING REACTIONS

by

GARY DALE WAIT

A THESIS

SUBMITTED TO THE FACULTY OF GRADUATE STUDIES

IN PARTIAL FULFILMENT OF THE REQUIREMENTS FOR THE DEGREE

OF MASTER OF SCIENCE

DEPARTMENT OF PHYSICS
EDMONTON, ALBERTA

September, 1964

THE UNVIERSITY OF ALBERTA

FACULTY OF GRADUATE STUDIES

The undersigned certify that they have read and recommend to the Faculty of Graduate Studies for acceptance a thesis entitled, "Studies of Some Deuteron Stripping Reactions," submitted by GARY DALE WAIT in partial fulfilment of the requirements for the degree of Master of Science.

ABSTRACT

The original purpose of the experiment was the determination of the contribution of exchange stripping in the $O^{17}(d,n)F^{18}$ reaction. However, the absolute cross section of the $O^{17}(d,p)O^{18}$ reaction was found to be so small as to discourage this. It was necessary to determine the angular distributions of $C^{12}(d,p)C^{13}$ and $C^{13}(d,p)C^{14}$ from a natural carbon target in order to get a measure of the angular distribution of $O^{17}(d,p)O^{18}$ since the C^{13} contamination swamped the peak from the O^{18} ground state. The absolute cross sections of $C^{12}(d,p)C^{13}$ and $C^{13}(d,p)C^{14}$ and $O^{17}(d,p)O^{18}$ were subsequently measured at bombarding energies of 1 and 1.5 Mev for comparison purposes. The angular distribution of $O^{16}(d,n)F^{17}$ was also measured at a bombarding energy of 3.5 Mev for comparison with the $O^{16}(d,p)O^{17}$ reaction.

ACKNOWLEDGEMENTS

I am indebted to my Supervisor, Dr. J. T. Sample, and Dr. G. C. Neilson and Dr. W. K. Dawson for their assistance throughout the period of my studies.

Thanks are due to Dr. T. K. Alexander for his suggestions during the early portion of the experiment and to Dr. W. C. Olsen, who was very helpful throughout the entire experiment. I am also indebted to Dr. B. Cujec for her valuable assistance and to Tsing Lam for his assistance in the setting up and operation of the experimental equipment.

I wish to thank Dr. W. K. Dawson, T. Grandy, and W. Davies for programming and operating the computer for the many calculations that were necessary.

Thanks also to J. B. Elliott, L. Holm, and E. B. Cairns for their assistance in keeping the equipment operational, and to G. Tratt for her assistance in drafting the thesis.

TABLE OF CONTENTS

LIST OF FIGURES

INTRODUCTION

In 1951 S. T. Butler (Bu 51) put forth his theory of the angular distribution of stripping reactions. From this theory experimentalists were given a new tool with which to probe the nucleus. The theory has not, however, explained satisfactorily all the experimental data available. The research reported in this thesis is part of a program to obtain a measure of the contributions of perturbing effects. Comparison of differential cross sections and polarizations of reaction products from the four reactions $O^{16}(d,p)O^{17}$, $O^{16}(d,n)F^{17}$, $O^{17}(d,p)O^{18}$ and $O^{17}(d,n)O^{18}$ will give at least a qualitative measure of the relative contributions of the possible reaction mechanisms.

Stripping reactions are direct reactions of the type X(a,f)Y where a is an incoming particle on a target nucleus X, f is an outgoing (free particle) and Y is the product nucleus from the reaction in a particular state. The particle a is made up of a particle f and a particle c (captured).

Direct reactions are those in which the transformation from the incident particle plus the target nucleus to the outgoing particle plus the final nucleus occurs directly. These reactions are to be compared with those in which the incident particle plus the target nucleus combine for a finite time to form a compound nucleus which then emits one or more of its nucleons.

In particular there are the deuteron stripping reactions. In Figure 1 A refers to the mass number of the target nucleus.

From the angular distributions of pure stripping reactions knowledge can be gained about the spin and parity of the different states of the final nucleus providing something is known of the initial nucleus.

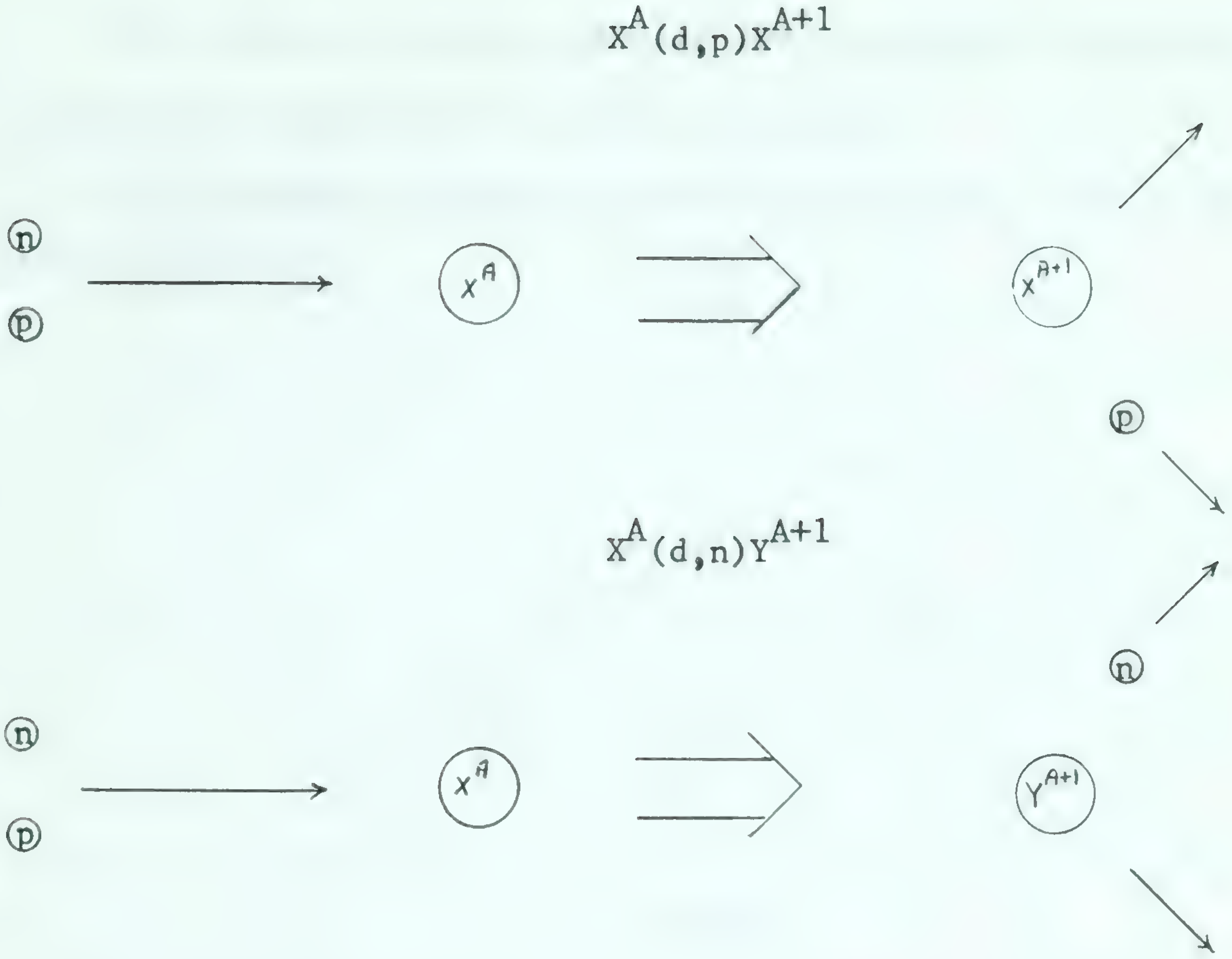

Figure 1

If the spins of the nuclei are $\vec{J}_x$ and $\vec{J}_y$ and the spin of c is S_c(=1/2), then the orbital angular momentum $\vec{\ell}_c$ satisfies the following vector equation.

$$\vec{J}_y = \vec{J}_x + \vec{\ell}_c + \vec{S}_c$$

or $$(J_x + J_y + 1/2) \geq \ell_c \geq \left| J_x + J_y + S_c \right| \text{ min.} \qquad (1)$$

The relation
$$\pi_y = \pi_x \pi_c (-1)^{\ell} \qquad (2)$$

must also hold, where π_y is the parity of the state of Y fed by the reaction, π_x is the parity of the ground state of X and π_c = +1 when c is a proton or a neutron.

The shape of the angular distribution depends largely on ℓ_c as can be seen from a simple semi-classical argument.

The momentum carried into the nucleus is $\hbar\vec{k}_y = \hbar\vec{k}_d - \hbar\vec{k}_f$ by conservation of momentum.

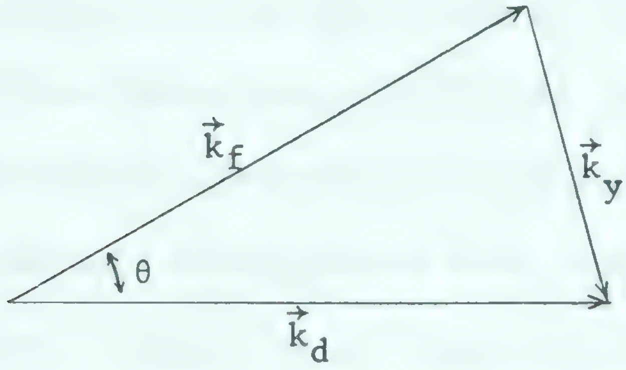

Figure 2

As can be seen from Figure 2, $|\vec{k}_y|$ is a minimum when $\theta = 0$.

The maximum orbital angular momentum carried into the nucleus is given by $\hbar|\vec{k}_y|r_o$ where r_o is the stripping radius of the target nucleus. Thus in order for the reaction to proceed the following must be satisfied.

$$\hbar|\vec{k}_y|\, r_o \geq \hbar\ell_c \tag{3}$$

Without this condition it is reasonable to assume that most of the outgoing particles would proceed in the forward direction. Thus for $\ell_c = 0$ the angular distribution would be peaked forward. For $\ell_c > 0$ equation 3 may not be satisfied at $\theta = 0$ and $|\vec{k}_y|$ would have to be increased. As is seen from Figure 2 $|\vec{k}_y|$ is increased as θ is increased and thus the angular distributions of higher ℓ_c values would be expected to "peak" at higher values of θ.

If the angular distribution is measured for a particular reaction and the spin and parity of the initial nucleus is known, then the spin and parity of the final state may be determined.

However, conditions must be ideal for the experimental data to fit the theory of pure stripping. There are other effects which tend to obscure the position of the peak. One of these is the contribution from compound nucleus formation in which the incident deuteron is captured by the target nucleus for a finite time and then particle f is emitted. The angular distribution from compound nucleus reactions would tend to be much flatter than those from stripping reactions. $\sigma(\text{compound nucleus}) = \sum_{n=0}^{\ell} A_n P_n(\theta)$ and any sharp peaks in such an angular distribution would require high values of ℓ. An effect of compound nucleus formation is the presence of resonances in the differential cross section corresponding to levels in $(X + d)^{A+2}$. Another important contribution comes from the presence of the coulomb field which tends to scatter the incident deuteron as well as the emerging particle if it happens to be the proton. This is shown in Figure 3.

Figure 3

The incident deuteron is scattered before the reaction in the direction $\vec{k}'_d$ and the outcoming proton is scattered further after the reaction. This causes the peak of angular distribution to be displaced to a more backward angle and to be smeared out because of the range of impact parameters possible in a given reaction.

In certain cases in which there is a loosely bound nucleon on the target nucleus, so-called exchange stripping reactions occur. These reactions are a special case of knock out reactions in which the incident particle knocks out a nucleon from the target and is then captured. In the case of exchange stripping reactions the incident deuteron interacts strongly at the surface with one of the nucleons. This nucleon is emitted and the deuteron is absorbed.

If the exchange reaction is prominent, then the angular distribution shows peaks not characteristic of pure stripping.

Semi-classically the angular distribution would exhibit maxima at angles for which

$$|\vec{L}| = |\vec{\ell}_o + \vec{\ell}| \leq |\vec{k}_y| r_o$$

(See Figure 2)

The maxima observed are not always limited to forward directions as for stripping but may just as easily appear in backward directions.

The limitations on L can be determined from

$$\vec{L} = \vec{J} + \vec{J}_o + \vec{S}_d + \vec{S}_f$$

or

$$|\vec{J} + \vec{J}_o + \vec{S}_d + \vec{S}_f|_{min} \leq L \leq J_o + J + S_d + S_f \qquad (4)$$

and

$$\pi_L = \pi_{Jo}\pi_J\pi_{Sd}\pi_{Sf} = \pi_{Jo}\pi_J \qquad (5)$$

The intrinsic spin of the deuteron is $|\vec{S}_d| = 1$. Thus it can be seen that in many cases L will be allowed more than one value whereas in the same reaction ℓ would have a specific value. Thus exchange stripping reactions could quite likely be detected if there were maxima showing in the angular distribution not predicted by Butler stripping theory.

Although a great deal of theoretical work has been done concerning stripping reactions, it is difficult to predict successfully absolute cross sections. However, it is useful to be able to compare ratios of cross sections expected from theory to those observed experimentally.

An important factor involved in the absolute cross section is

$$\frac{2J_f + 1}{2J_o + 1}$$

For example, when finding the ratio of the absolute cross section of $O^{16}(d,p)O^{17}$ to $O^{17}(d,p)O^{18}$ the above factor gives rise to a 36 to 1 ratio in cross section. Essentially this arises because of the following. In the case of $O^{16}(d,p)O^{17}$, $J_o^{\pi} = 0^+$ and $J_f^{\pi} = 5/2^+$. Thus two units of angular momentum are carried in by the captured neutron. In the case of $O^{17}(d,p)O^{18}$, $J_o^{\pi} = 5/2^+$ and $J_f^{\pi} = 0^+$ and two units are carried in

again by the captured neutron. However, in the second case the direction of the angular momentum must be chosen to just cancel the orbital angular momentum of the initial nucleus.

The absolute cross section is proportional as well to the reduced width of the level involved. However, this involves detailed knowledge of the internal wave functions of the nuclei involved. The reduced width is defined as

$$\gamma_{\ell c} = \frac{\hbar^2}{2m_c^* q r_o} \left| f_o(J, J_o, \ell_c; r_o) \right|^2 \qquad (6)$$

Where $|f_o(J,J_o,\ell_c;r_o)|^2$ is the probability density for finding the captured particle at $r = r_o$ of the final nucleus with $\ell = \ell_c$, and m_c^* is the reduced mass of the nucleus and q is a number which is defined later. One would not expect values of $|f_o(J,J_o,\ell_c;r_o)|^2$ from two similar nuclei to differ by much more than a factor of two.

The ratio between the two cross sections is

$$\frac{\frac{d\sigma_1}{d\omega}}{\frac{d\sigma_2}{d\omega}} = \frac{r_{01}^2\ (2J_{f_1}+1)(2J_{o_2}+1)\sqrt{E_{f_1}}\ |f_{o_2}|^2 \sigma^{\ell}_{TAB_1}}{r_{o_2}^2\ (2J_{o1}+1)(2J_{f_2}+1)\sqrt{E_{f_2}}\ |f_{o_2}|^2 \sigma^{\ell}_{TAB_2}} \qquad (7)$$

The factor σ^{ℓ}_{TAB} contains all of the angular dependence. The magnitude of σ^{ℓ}_{TAB} tends to be larger at smaller angles with the restriction $|\vec{k}_y| \geq \hbar\ell_c$ which for $\ell_c > 0$ usually causes a peak in the angular distribution for $\theta > 0$.

BUTLER STRIPPING

Before beginning the discussion of Butler theory the conditions for its validity should be stated. There are three main approximations, the first of which is the neglect of the interaction V_{xf} between the initial nucleus and the particle f. The second approximation neglects the interaction between the neutron and proton, that constituted the deuteron, after one of these has penetrated into the target nucleus. Neglect of elastic and inelastic scattering of the incident deuteron is the third approximation. The three approximations should be quite accurate for large deuteron impact parameters such that particle f passes the target nucleus at some distance.

The initial nucleus is assumed to be confined within a sphere of radius r_o. Thus for $r_c > r_o$ particle c does not interact with the nucleus and for $r_c < r_o$ particle c interacts strongly with the nucleus.

The wave function describing the system for $r_c < r_o$ can be written as a Fourier expansion (Bu 57):

$$\psi_{rc<ro} = \chi_f(\mu_f') \int B(J_o, M_o, \mu_d, \mu_f', M; \vec{k}_f) v(M; \vec{r}_c, S_c, \xi; k_f) \times e^{i\vec{k}_f \cdot \vec{r}_f} d\vec{k}_f \quad (8)$$

where the spin function $\chi_f(\mu_f') = \delta_{\mu f\ \mu f'}$

μ_f is the z-projection of the spin of particle f and the prime on μ_f' and any other symbol is meant to indicate that the quantities pertain to outgoing channels.

M_o is the z-projection of the spin, J_o of the target nucleus. M is the z-projection of the spin of the initial nucleus plus the captured particle c.

$$\vec{k}_f = \frac{2m}{\hbar^2}(E_f)^{1/2}$$

is the wave vector of the free particle f. ξ represents all coordinates of the particles of the initial nucleus. $B(J_o, M_o, \mu_d, \mu_f', M; \vec{k}_f)$ is the amplitude factor to be determined from boundary conditions. $e^{i\vec{k}_f \circ \vec{r}_f}$ is a plane wave describing the emission of particle f and v is a solution of

$$\frac{\hbar^2}{2m_c^*} \nabla_c^2 v + (E_c - V(r_c))v = 0 \tag{9}$$

normalized such that

$$\int_{r_c \leq r_o} |v|^2 d\vec{r}_c \; d\xi \; dS_c = 1 \tag{10}$$

where $E_c = E_d - \varepsilon_d - E_f$ and $m_c{}^* = \dfrac{m_c m_I}{m_c + m_I}$

is the reduced mass of particle c with respect to the initial nucleus. All quantities are to be considered to be in center of mass coordinates.

For convenience of boundary matching the following expansion is made.

$$v(M; \vec{r}_c, S_c, \xi, k_f) = \sum_{\alpha, M_\alpha, \Lambda_c'} \mu_\alpha(J_\alpha, M_\alpha, \xi) \; \chi_c(\mu_c') \; Y_{\ell_c'}^{m_c'}(\theta_c, \theta_c) \times \frac{f_\alpha(M, J_\alpha, M_\alpha, \Lambda_c'; k_f, r_c}{r_c} \tag{11}$$

in which μ_α is the normalized wave function of the state α of the initial nucleus. $\Lambda_{c'}$ refers to $(\ell_{c'}, m_{c'}, \mu_{c'})$ and f_α, it turns out, is related to the reduced width.

For the region $r_c > r_o$ the wave function has the form

$$\psi_{rc>ro} = \chi_f(\mu_{f'}) \sum_{\alpha, M_\alpha, \Lambda_{c'}} \mu_\alpha(J_\alpha, M_\alpha, \xi) Y^{m_{c'}}_{\ell c'}(\theta_c, \phi_c) \chi_c(\mu_{c'})$$

$$\times \int A(J_o, M_o, J_\alpha, M_\alpha, \mu_\alpha, \Lambda_{cf'}, M; \vec{k}_f) \; \kappa_\alpha h^{(1)}_{\ell c'}(i\kappa_\alpha r_c)$$

$$\times \; e^{i\vec{k}_f \circ \vec{r}_f} \, d\vec{k}_f \; + \; \mu_o(J_o, M_o, \xi) \sum_{\Lambda_{cf}} \chi_c(\mu_c) \; \chi_f(\mu_f) Y^{m_c}_{\ell c} (\theta_c, \phi_c)$$

$$\times \int \Phi(\Lambda_{cf}, \mu_d, k_f, r_o) \; e^{i\vec{k}_f \circ \vec{r}_f} \, d\vec{k}_f \tag{12}$$

The first term describes particle f and c as both being free, whereas the second term describes the incoming plane wave motion of the deuteron. $r_c \times h'_{\ell c}(i\kappa r_c)$ is the radial wave function describing the motion of a freely moving particle c with angular momentum $\ell_{c'}$ and energy $\frac{\hbar^2}{2m}(i\kappa_\alpha)^2$. The spherical Hankel function is defined as

$$h^{(1)}_\ell(i\kappa r) = \frac{e^{-\kappa r}}{\kappa r} \sum_{n=o}^{\ell} \frac{(\ell + n)!}{n!(\ell-n)!} (2\kappa r)^{-n}$$

If κ_α is real, the particle c is considered to be captured with a negative energy into a bound state. The amplitude factor A is to be determined from the boundary conditions.

Λ_{cf}' represents (Λ_c', μ_c').

Φ is the so-called stripping transform.

The boundary conditions necessary for a solution are that the wave functions join smoothly at $r_c = r_o$, i.e.

$$\left[\psi \; r_c < r_o\right]_{r_c=r_o} = \left[\psi \; r_c > r_o\right]_{r_c=r_o} \tag{13}$$

and

$$\left[\frac{d\psi}{dr_c} \quad r_c < r_o\right]_{r_c=r_o} = \left[\frac{d\psi}{dr_o} \quad r_c > r_o\right]_{r_c=r_o} \tag{14}$$

The boundary conditions imply that in the neighbourhood of $r = r_o$ that

$$f_\alpha(M, J_\alpha, M_\alpha, \Lambda_c'; k_f r_c) = a_\alpha(M, J_\alpha, M_\alpha, \Lambda_c'; k_f)$$

$$\times \quad \kappa_\alpha r_c h'_{\ell c'}(i\kappa_\alpha r_c) + \delta_{\alpha,o}\, \delta_{M\alpha,Mo}\, \delta_{\Lambda_c'\Lambda_c}\, b_o(M, J_o, M_o, \Lambda_c; k_f) h^{(2)}_{\ell_c'}(i\kappa_o r_c)\kappa_o r_c \tag{15}$$

where $h^{(2)}_\ell(i\kappa r) = \dfrac{e^{\kappa r}}{\kappa r} \displaystyle\sum_{n=o}^{\ell} \dfrac{(\ell + n)!(-2\kappa r)^{-n}}{n!\;(\ell - n)!}$

It can be seen that if any of the quantities in the Dirac data functions of Equation 7 cause the second term to be zero, then f_α is the radial wave function describing c as a free particle. However, when c is captured into a particular state E_c then the radial function f_α must decrease exponentially for $r > r_c$ and thus $b_o = 0$.

On substitution of the values of B and f_α into Equation 8 and A and f_α into Equation 12, it is found that 8 and 12 are identical for large values of r_f.

The theorem of Residues is used and integration carried out around appropriate contours containing the zeros which arise from b_o being zero in an eigenstate B_o. The assymptotic form of the wave function is

$$\psi \xrightarrow[r_f \to \infty]{} 2\pi^2 \sum_{\Lambda cf} \delta\mu_{f}, \mu_{f'} \chi(\mu_{f'}) \sum_{\beta} \frac{e^{i\kappa_{f\beta} r_{f\beta}}}{\kappa_\beta \, r_f} k_{f\beta} \, v_\beta(J_\beta, M, \xi, \vec{r}_c)$$

$$\times \; W\{\Phi(\Lambda_{cf}; \kappa_{f\beta}, r_c), \; \kappa_o r_c h^{(1)}_{\ell_c}(i\kappa_\beta r_c)\}_{r_c = r_o}$$

$$\times \; \{a_o(J_\beta, M, J_o, M_o, \Lambda_c; k_{f\beta}) \times \frac{d}{d_{k_{f\beta}}} \; b_o(J_\beta, M, J_o, M_o, \Lambda_c; k_{f\beta})\}^{-1} \tag{16}$$

where

$$W(A,B) = B \frac{\partial A}{\partial r_c} - A \frac{\partial B}{\partial r_c}$$

is the Wronskian of A and B. The cross section for the capture of particle c in a particular state is thus

$$\sigma(\theta_f) = \frac{4\pi^4 \, k_f^3 \, m_d^* \, q}{m_f^* \, k_d \, \kappa_o} \; \frac{2J + 1}{2(2J_o + 1)} \sum_{\ell_c m_c} \frac{1}{(2\ell_c + 1)} \left| N(J, J_o, \ell_c) \right|^2$$

$$\times \; \left| W(\Phi(\ell_c, m_c; \vec{k}_f, r_c), \; \kappa_o r_c \; h^{(1)}_{\ell_c} \; (i\kappa_o r_c))_{r_c = r_o} \right|^2 \tag{17}$$

where

$$q = \int \left| v_\beta \right|^2 d \; \xi dr_c ds_c$$

which is slightly greater than unity because of normalization of v.

$$N = \left\{ a_o \frac{db_c}{dk_f} \right\}^{-1}$$

and Φ is the stripping transform.

The sum over ℓ_c is subject to the following restrictions:

$$|\vec{J} + \vec{J}_o + \vec{S}c|_{min} \leq \ell_c \leq J + J_o + 1/2$$

and

$$\pi_{J_o} = \pi_J (-1)^{\ell}$$

Using

$$\chi(|\vec{r}_f' - \vec{r}_c|) \, e^{\frac{i\vec{k}d}{2} \circ (\vec{r}_f' + \vec{r}_c)} = \sum_{\ell_c m_c} Y_{\ell_c}^{m_c *}(\theta_c, \phi_c)$$

$$\text{x} \int \frac{\Phi(\ell_c, m_c ; \vec{k}_f \circ r_c)}{r_c} \, e^{i\vec{k}_f' \circ \vec{r}_f'} \, d\vec{k}_f' \tag{18}$$

where

$$\vec{r}_f' = \vec{r}_f + \frac{m}{m_f} \vec{r}_c$$

it follows that

$$\Phi(\ell_c, m_c; \vec{k}_f, r_c) = \frac{r_c}{(2\pi)^3} \int d\phi_c d\theta_c \sin\theta_c Y_{\ell c}^{m_c^*} \, e^{i \frac{m}{m_f} \vec{k}_f \circ \vec{r}_c}$$

$$\text{x} \int d\vec{r}_f' \, \chi(|\vec{r}_f' - \vec{r}_c|) \, e^{\frac{i\vec{k}d}{2} (\vec{r}_f' + \vec{r}_c')} \, e^{-i\vec{k}_f \circ \vec{r}_f'} \tag{19}$$

where r_f' is the coordinate of particle f with respect to the center of mass of the initial nucleus. Using the Hulthen function for χ which is

defined as

$$\chi(r) = \frac{\left(\frac{1}{2\gamma} - \frac{\rho_t}{2}\right)^{-1/2}}{\sqrt{4\pi}\ \ r} \left\{e^{-\gamma r} - e^{-\zeta r}\right\} \tag{20}$$

and the reduced width

$$\gamma_{\ell c} = \frac{\hbar^2}{2m_c{}^*qr_o} \{\kappa_o r_o h_\ell^{(1)}(i\kappa_o r_o)\}^2 \ \frac{q\ m_c^*\ k_f}{m_f{}^*\ \kappa_o}{}^{2} \left|N(J,J_o\ell_c)\right|^2 \tag{21}$$

the cross section becomes

$$\sigma(\theta_f) = \frac{\left(\frac{1}{2\gamma} - \frac{\rho_t}{2}\right) r_o\ m_d{}^*\ m_f{}^*}{\hbar^2\ m_c{}^*} \ \frac{k_f}{k_d} \left(\frac{2J+1}{2J_o+1}\right) \left\{\frac{1}{K^2+\gamma^2} - \frac{1}{K^2+\zeta^2}\right\}^2$$

$$\times \sum_{\ell c} \gamma_{\ell c} \left| W\left\{ j\ (Qr_c),\ \frac{h_{\ell c}^{(1)}(i\kappa_o r_c)}{h_{\ell c}^{(1)}(i\ \kappa_o r_o)} \right\}_{r_c=r_o} \right|^2 \tag{22}$$

where

$$\vec{Q} = \vec{k}_d - \frac{m_i}{m_f}\ \vec{k}_f$$

and the m*'s are the reduced masses.

$$K = \left|\frac{\vec{k}_d}{2} - \vec{k}_f\right|$$

$$\gamma^2 = \frac{m}{\hbar^2}\varepsilon_d$$

where ε_d is the deuteron binding energy. ρ_t is the triplet effective range.

COULOMB CORRECTIONS

For addition of coulomb effects the three wave functions are generalized as follows:

$$e^{i\vec{k}_f \cdot \vec{r}_f} \longrightarrow \psi_f(\vec{k}_f, \vec{r}_f)$$

$$\kappa_o r_o h_\ell^{(1)}\,(i\kappa r_o) \longrightarrow g_\ell^{(1)}(i\kappa_o r_o)$$

$$\Phi(\ell_c, M_c; \vec{k}_f, r_c) \longrightarrow \overset{s}{\Phi}\,(\ell_c, M_c; \vec{k}_f, r_c)$$

where $\psi(\vec{k}_f, \vec{r}_f)$

is a solution of

$$\left\{ \frac{\hbar^2}{2m_f{}^*} \nabla^2{}_f + \frac{\hbar^2}{2m_f{}^*}\, k_f^2 - \frac{Ze^2\ \varepsilon(f)}{r_f} \right\} \psi(\vec{k}_f, \vec{r}_f) = 0 \tag{23}$$

where $\varepsilon(p) = 1$ and $\varepsilon(n) = 0$

Thus if f is a neutron $\varepsilon(f) = 0$ and

$$\psi(\vec{k}_f, \vec{r}_f) = e^{i\vec{k}_f \cdot \vec{r}_f}$$

$$g_{\ell}^{(1)}(i\kappa r_o)$$

is a solution of

$$-\frac{d^2 g_{\ell}^{(1)}}{dr^2} + \kappa^2 g_{\ell}^{(1)} + \frac{2m_c^*}{\hbar^2}\left\{\frac{\ell(\ell+1)}{r^2} + \frac{Ze^2}{r}\varepsilon(c)\right\} g_{\ell}^{(1)} = 0 \qquad (24)$$

Thus if c is a neutron $\varepsilon(c) = 0$ and

$$g_{\ell}^{(1)}(i\kappa r) = \kappa r\, h_{\ell}^{(1)}(i\kappa r)$$

$\Phi^s(\ell_c, m_c; \vec{k}_f, r_c)$ is expanded in terms of $\psi(k_f, r_f)$ rather than $e^{i\vec{k}_f \cdot \vec{r}_f}$ and $e^{\frac{i\vec{k}_d}{2} \cdot (\vec{r}_f + \vec{r}_c)}$ is replaced by the solution ψ_d which is analagous to $\psi(\vec{k}, \vec{r}_f)$, the solution of Equation 23.

Thus with the above substitutions Equation 17 becomes

$$\sigma(\theta_f) = \frac{4\pi^4 k_f^3 m_d^* q}{m_f^* k_d \kappa_o^2} \frac{2J+1}{2J_o+1} \sum_{\ell_c m_c} \frac{1}{(2\ell_c+1} \left|N(J, J_o, \ell_c)\right|^2$$

$$\left|W\{\Phi^s(\ell_c, m_c; \vec{k}_f, r_c), g_{\ell c}^{(1)}(i\kappa_o r_c)\}\right|^2 \qquad (25)$$

Now all that is necessary is to determine the form of these more general functions. The solution of 23 is of the form

$$\psi(\vec{k}_f, \vec{r}_f) = 4\pi \sum_{\ell, m} i^{\ell} e^{-i\sigma_{\ell}} \frac{F_{\ell}(k_f r_f)}{k_f r_f} Y_{\ell}^m(\theta_f, \phi_f) Y_{\ell}^m(\theta, \phi) \qquad (26)$$

where
$$\frac{F_\ell(k_f r_f)}{k_f r_f} \longrightarrow \frac{\sin}{k_f r_f}\left(k_f\, r_f - \eta_f \log 2\, k_f r_f - \frac{\ell\pi}{2} + \sigma_\ell\right)$$

are the regular coulomb functions which are just

$$j_\ell(k_f r_f) \text{ for } \xi(f) = 0$$

σ is the coulomb phase shift and $\eta_f = \dfrac{Ze^2 m_f^*}{\hbar^2 k_f}$.

Similarly
$$\psi_d(\vec{k}_d,\vec{r}_f,\vec{r}_c) = \chi(|\vec{r}_c-\vec{r}_f|) \sum_L i^L e^{i\sigma_L} (2L+1) \frac{F_L(k_d R)}{k_d R} P_L(\cos\theta) \tag{27}$$

where $\vec{R} = \dfrac{\vec{r}_f + \vec{r}_f}{2}$ and θ is the angle between $\vec{R}$ and $\vec{k}_d$.

The stripping transform

$$\Phi^s(\ell_c, m_c; \vec{k}_f, r_c) = \frac{r_c}{(2\pi)^3} \int \sin\theta_c\, d\theta_c\, d\phi_c\, Y_{\ell_c}^{m_c}(\theta_c,\phi_c) \times \int dr_f\, \psi_d(\vec{k}_d,\vec{r}_f,\vec{r}_c)\, \psi_f^*(\vec{k}_f,\vec{r}_f) \tag{28}$$

can now be used directly to evaluate

$$W(\Phi^s, g_\ell)$$

The use of Green's theorem and the wave equations involved plus the zero range approximation

$$V_{cf}\chi(|\vec{r}_f-\vec{r}_c|) = \frac{-\hbar^2\sqrt{8\pi\gamma}}{m}\,\delta(\vec{r}_f - \vec{r}_c)$$

gives the result

$$W\left\{\Phi^{s}_{\ell_c m_c},\ g^{(1)}_{\ell_c}\right\} = \frac{-4\pi\sqrt{2\pi\gamma}}{(2\pi)^3} \int_{r_c \geq r_o} d\vec{r}_c\ \frac{g^{(1)}_{\ell_c}(i\kappa r_c)}{r_c}$$

$$\times\ \psi_f^{*}\ (\vec{k}_f, \vec{r}_f)\ \ \psi_d(\vec{k}_d, \vec{r}_f, \vec{r}_c) \qquad (29)$$

Substituting ψ_d from Equation 27 and ψ from Equation 26 yields, after the angle integrations are carried out,

$$W\left\{\Phi^{s}_{\ell_c, m_c},\ g^{(1)}_{\ell_c}\right\}_{r_c = r_o} = \frac{-16\pi}{(2\pi)^3}\ \frac{\sqrt{2\pi\gamma}}{k_d k_f} \sum_{\ell, L, m} Y^{m}_{\ell}\ (\theta,\phi)(2L+1)$$

$$\times\ \left(\frac{2\ell + 1}{2\ell_c + 1}\right)^{1/2}\ i^{L-1}\ e^{i(\sigma_\ell + \sigma_L)}\ C_{\ell L}(\ell_c, 0; 0, 0)\, C_{\ell L}(\ell_c, m_c; m, 0)$$

$$\times \int_{r_o}^{\infty} \frac{g^{(1)}_{\ell_c}(i\kappa r)}{r}\ \ F_\ell(k_f r)\ F_L(k_d r)\ dr \qquad (30)$$

The evaluation of Equation 30 is obviously much more involved than that of a term like $W(j_\ell, h_\ell^{(1)})$ and a great deal of laborious numerical calculation is necessary. In the case of (d,p) reactions the calculations involved in Equation 30 are greatly simplified since $g_\ell^{(1)}\ (i\kappa r_c)$ can be replaced by $h_\ell^{(1)}\ (i\kappa r_c)$. However, for (d,n) reactions

$$g_\ell^{(1)}(i\kappa r_c) = \ [F_{\ell_c}(i\kappa r_c) - iG_{\ell_c}(i\kappa r_c)]\ e^{-i\sigma_\ell}\ i^{\ell_c} \qquad (31)$$

A reasonable approximation of 31 for $\kappa' r_o >> 1$ is

$$g_\ell^{(1)}(i\kappa r_c) \simeq g_\ell^{(1)}(i\kappa' r_c)$$

where
$$(\kappa')^2 = \kappa^2 + \frac{2m^*_c}{\hbar^2}\,\frac{Ze^2}{r_o}$$

which greatly simplifies calculation of Equation 30.

In general the coulomb interactions decrease the absolute cross section (especially for high L values) and also displace the maxima of the angular distributions to larger angles. However, in many cases the nuclear interactions, which are of an attractive nature, counteract the coulomb interactions and the position of the peak is moved to more forward angles.

EXPERIMENTAL ARRANGEMENT

The source of deuterons for the (d,p) stripping reactions was an High Voltage Engineering horizontal 2 Mev Van de Graaff. It was found convenient to run at 1.0 Mev and 1.5 Mev as the accelerator tube had aged and could not be run at higher energies. The beam was focused onto the desired target through four beam defining slits. The versatile target pot designed by J. B. Elliott for future use with a magnetic spectrometer allowed for vertical and horizontal displacement of the target as well as angular displacement with respect to the beam.

A solid state detector was mounted in the "exit port" of the target holder. It could easily be moved continuously to any angle from -135° to 135° and be positioned at any desired distance from the center of the target to a maximum of about 1-1/4".

For some runs a second detector was fixed in position at $\theta = -90°$ as a monitor while the first detector was moved from 0 to +135° measuring angular distributions.

It was found necessary to place thin foils in front of the detectors to stop scattered deuterons from entering at forward angles. Without these foils the detectors would soon have been destroyed because of the high deuteron flux.

The detectors were collimated with a piece .005" tantalum with a 0.040" diameter hole in the center. The solid angle of the effective detector surface was easily measured.

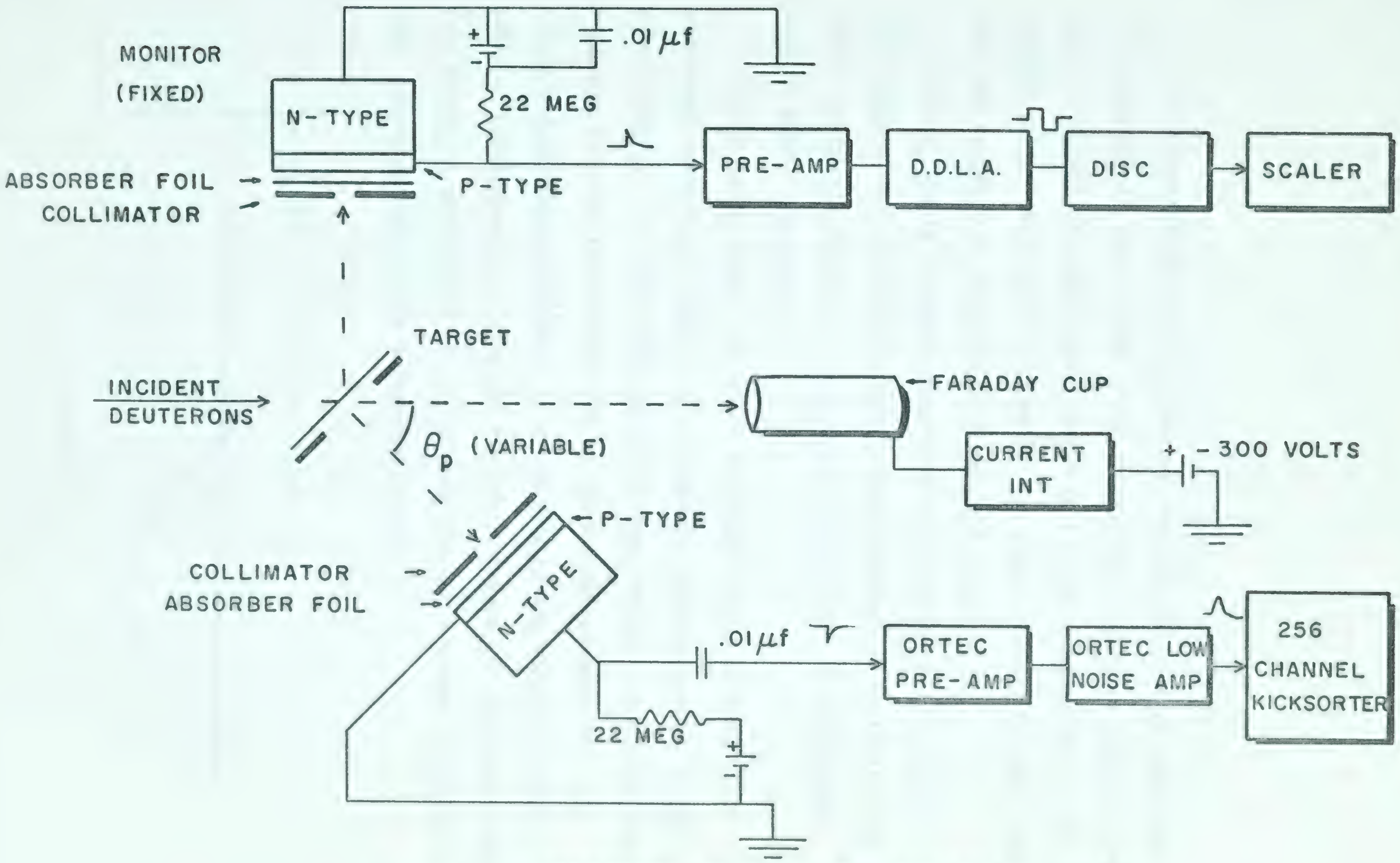

Figure 4. CHARGED PARTICLE SPECTROMETER

An alternate method of monitoring the beam was that of measuring the intensity of the .871 Mev γ ray emitted from the first excited state in O^{17}. A 6342 photomultiplier tube with a 2" NaI crystal was set up outside of the target pot. A "window" was placed on the .871 Mev γ ray peak and counts from this peak were fed to a scaler.

The $O^{16}(d,n)F^{17}$ angular distribution was obtained at a bombarding energy of 3.5 Mev with the High Voltage Engineering vertical 6 Mev Van de Graaff accelerator. The neutron energies were obtained using time of flight techniques.

The deuteron beam is pulsed at the high voltage terminal in 10 nanosecond bursts at a rate of 10^6/sec and is then accelerated to the desired energy. The analyzing magnet deflects the beam into a horizontal plane and the beam is then diverted by the switching magnet into the Mobley magnet bunching system. This bunching system consists essentially of two deflection plates and the Mobley magnet. A 10 megacycle/sec. r.f. signal is phased with the pulsed beam through a pickup in the drift tube, and is applied to the deflection plates.

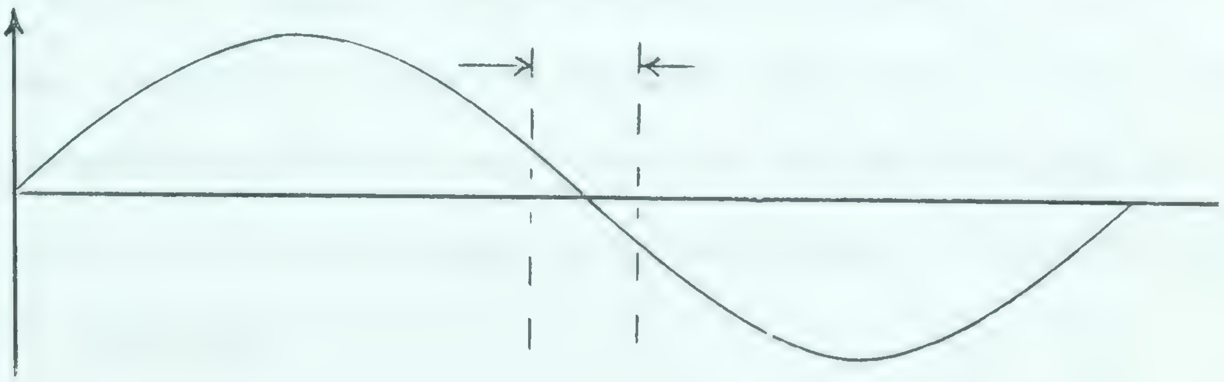

Figure 5

The portion of the cycle from a to b (Figure 5) is used to sweep the beam burst. This consists of one 10 nanosecond interval for each 10 cycles of the 10 megacycle signal. As is shown in Figure 6 the orientation of the beam burst is changed before entering the Mobley magnet.

The beam undergoes a deflection of 90° in the Mobley magnet and is focused at point f on the target. The portion of the burst that takes path a has farther to go than the portion taking path b. If the amplitude and phasing of the r.f. deflection are properly set, then the tail end of the burst overtakes the leading end of the burst giving a 1 nanosecond, or shorter, burst of deuterons at the focus.

With the beam properly pulsed, neutron time of flight measurements were carried out. A block diagram of the electronics is shown in Figure 7.

The neutron monitor was set at approximately one meter from the target at a fixed angle of $\theta_N = 60°$. The neutron peak arising from F^{17} ground state was integrated for normalization.

The liquid scintillator was set at a flight path of 6 meters and the spectrum from $O^{16}(d,n)F^{17}$ obtained in 15° intervals up to 90°. At a bombarding energy of 3.5 Mev the neutrons from the $O^{16}(d,n)F^{17}$ reaction were not detected at backward angles because the recoil of the final F^{17} nucleus reduces the neutron energy below the region of reliable operation of the spectrometer.

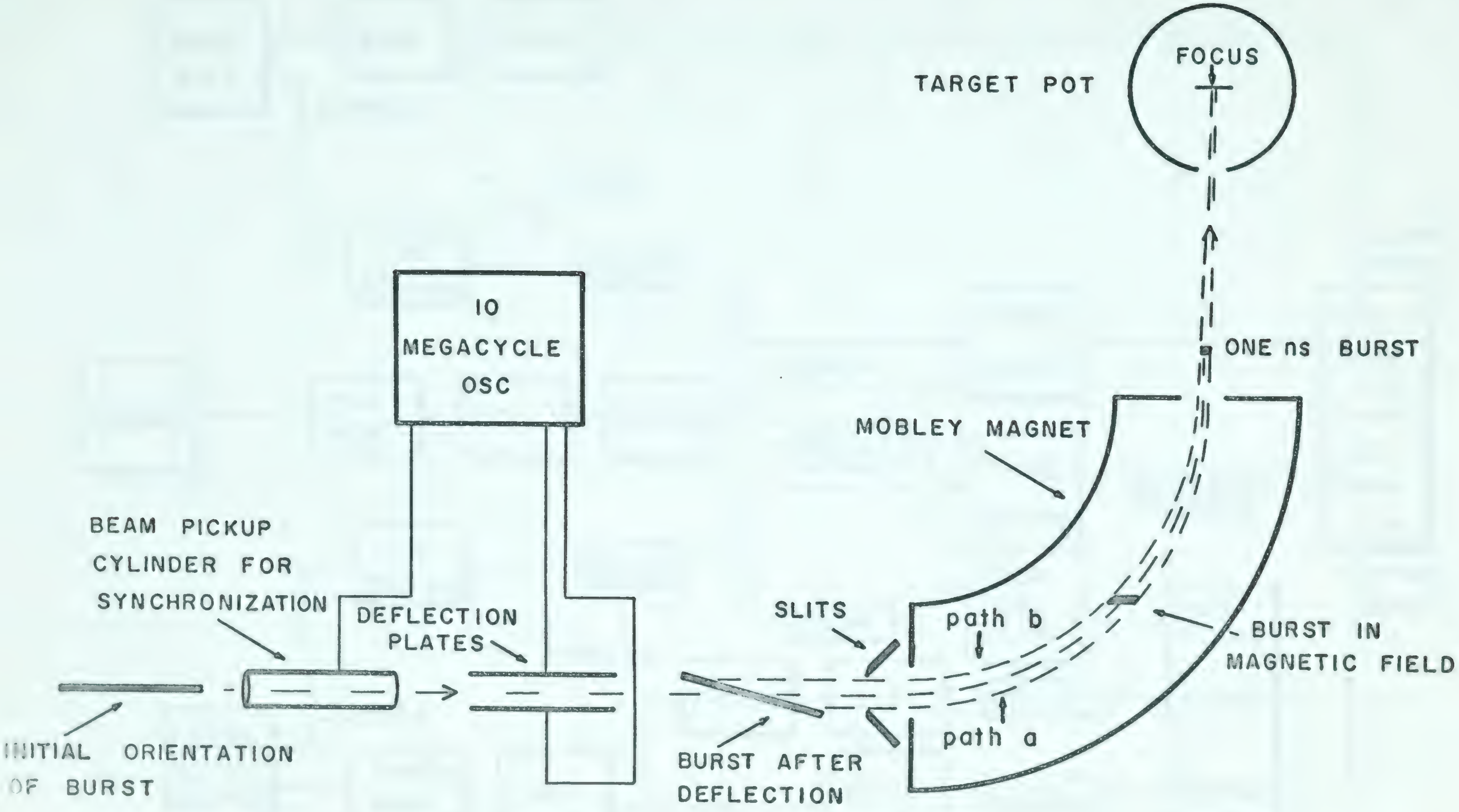

Figure 6. MOBLEY MAGNET BEAM BUNCHING SYSTEM

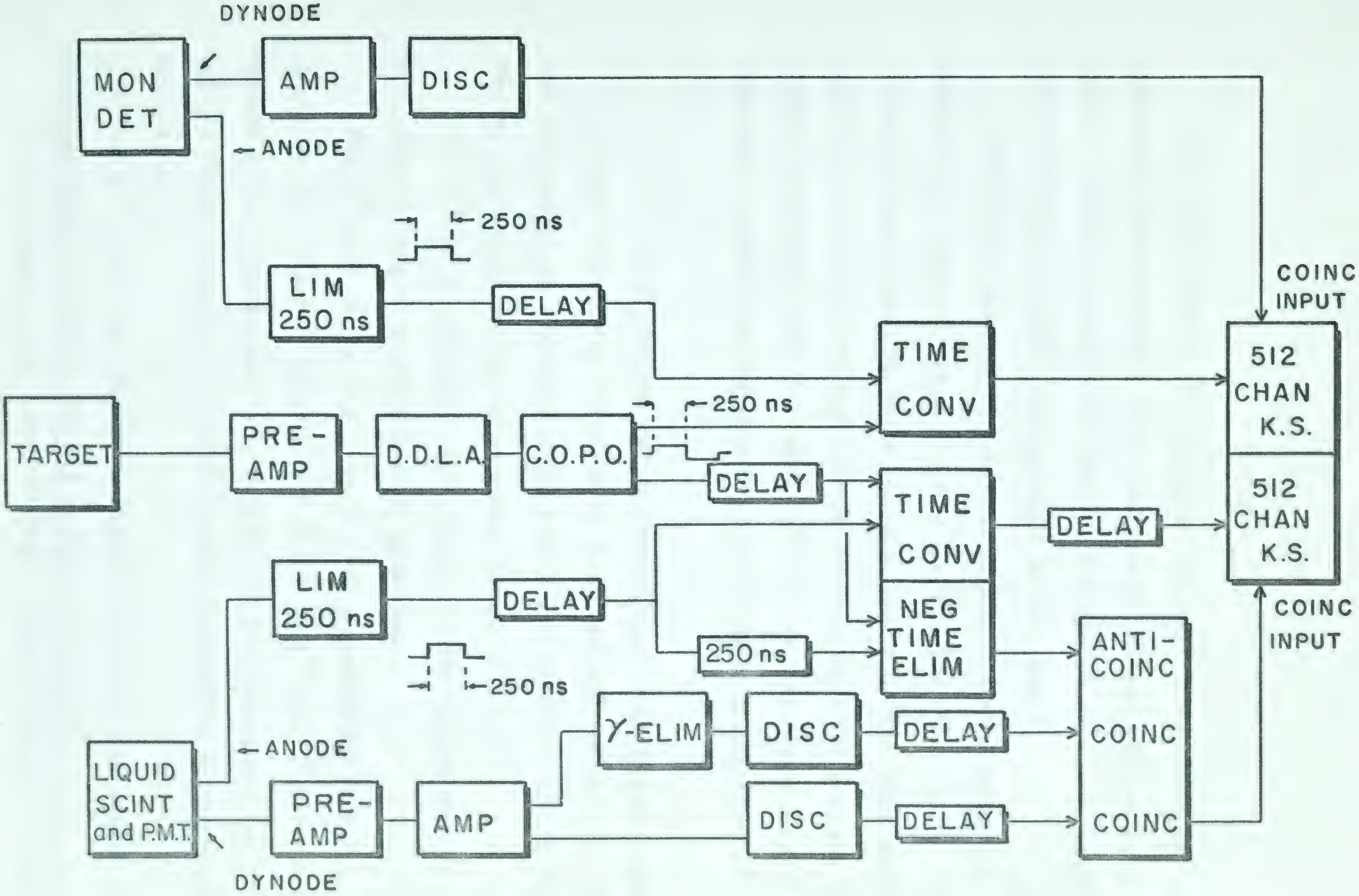

Figure 7. NEUTRON TIME OF FLIGHT SPECTROMETER

The target used in the reaction $O^{16}(d,p)O^{17}$ was a thin SiO_2 target prepared by heating quartz tubing and blowing several bubbles until they burst. A good thin sample was selected and mounted on a nickel target holder which had a (1/2") diameter hole in the center.

The natural carbon target was prepared on a thin 20 microinch nickel foil. The foil was placed over a 1/4" square hole cut in a piece of cardboard and a burning match was held under the hole. The unburned carbon from the match was deposited on the foil until the foil was completely blackened. Several targets were made in this manner for the purpose of checking the consistency of the relative abundance of C^{12} and C^{13}.

The O^{17} target was prepared at Harwell* in a mass spectrograph. O^{17} ions were accelerated and embedded in a 0.000025" nickel foil. This foil was mounted on a nickel backing with a 1/2" diameter hole in the center. The target was quoted as being 111 μgm/cm^2 of O^{17}.

The B^{10} target was a thin target prepared for earlier work by W. C. Olsen by use of a vacuum chamber evaporator.

The O^{16} used in the (d,n) reaction was a contaminant on a Be^9 target as well as a Si^{30} target. The levels in B^{10} and P^{31} were being studied by W. K. Dawson and G. C. Neilson and they suggested that the angular distributions of $O^{16}(d,n)F^{17}$(ground and .500) be extracted from their data.

The C^{13} target was prepared at Harwell using the same method described for O^{17}. The loading was quoted as 45 μgm/cm^2.

---

*Atomic Energy Research Establishment, Harwell, Berks., England.

ANALYSIS OF DATA

The reaction $B^{10}(d,p)B^{11}$ was used for energy calibration purposes. This was prompted by the fact that many levels in B^{11} appear in the proton spectrum and that reference could be made to W. C. Olsen's thesis for purposes of identifying the peaks. Since absorber foils were used the energy scale was non linear so that a comparison with other data was necessary.

The energy loss of charged particles in aluminium is plotted against thickness of aluminium in Figure 8 (Wh 58 and Ri 54). The amount of Al foil required to stop the scattered deuterons was estimated from Figure 8.

The spectrum from the reaction $B^{10}(d,p)B^{11}$ is shown in Figure 9. A PH-2-25-10 Nuclear Diodes* solid state detector was used with a stopping foil of 3.2 mgm/cm^2 Al. The calibration curve obtained (see Figure 10) was then used to define the proton groups from the O^{17} target (see Figures 11 and 12) when it was bombarded by 1.0 and 1.5 Mev deuterons.

It was found that a peak corresponding to the C^{14} ground state lay in the same channels as the O^{18} ground state peak. As there was

---

*Nuclear Diodes Inc., 1640 Old Deerfield Road, Highland Park, Illinois.

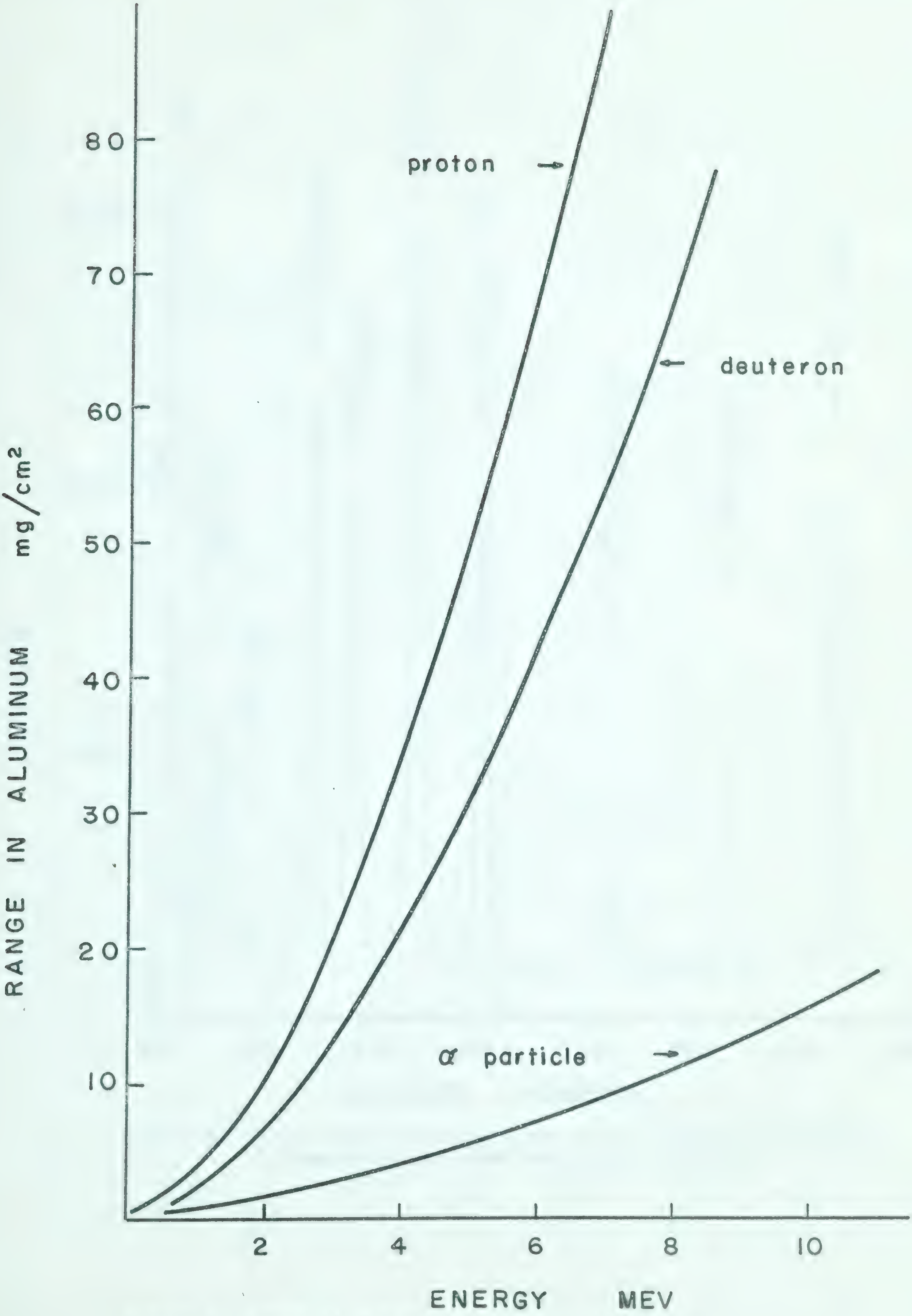

Figure 8. Range of Charged Particles in Aluminium.

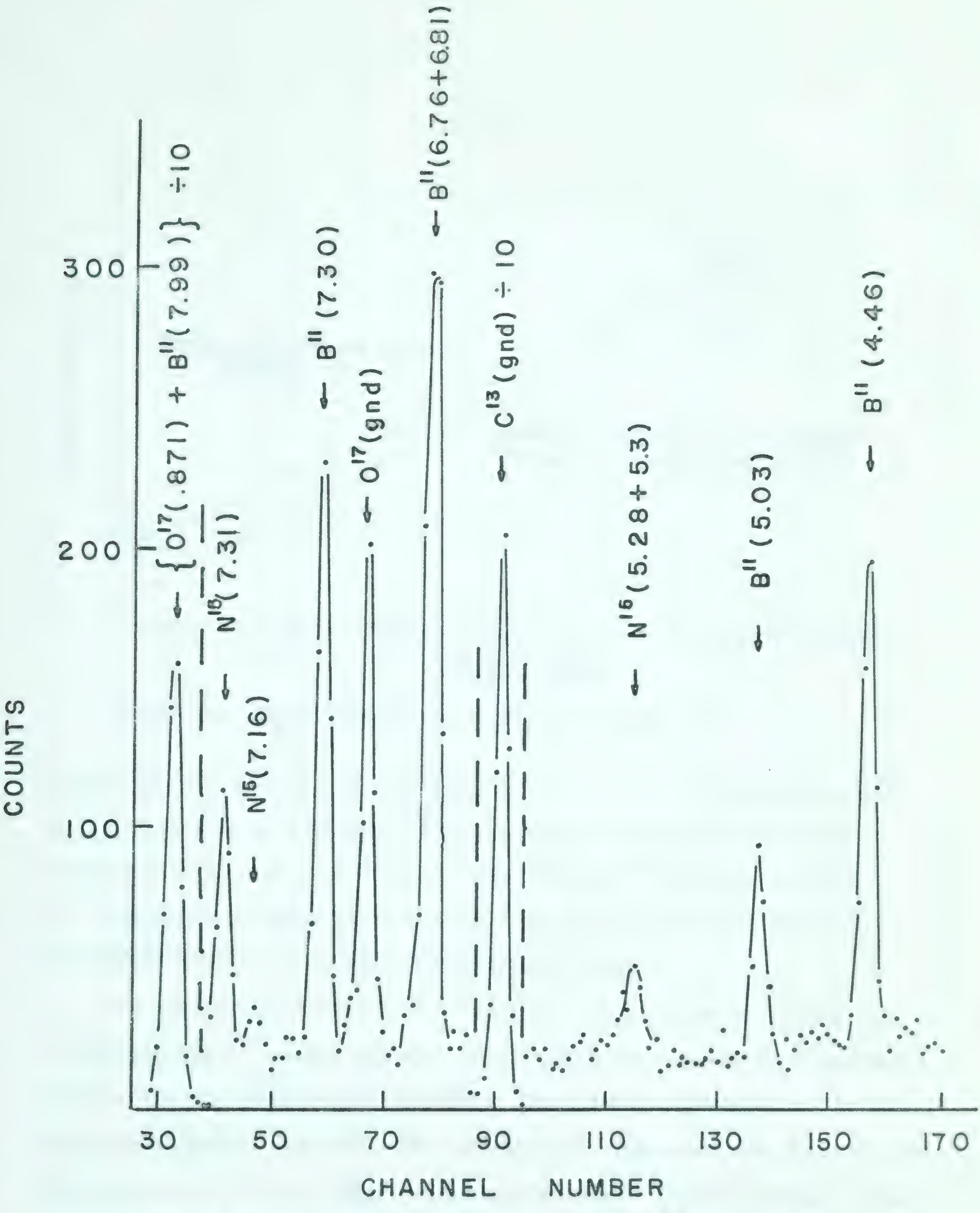

Figure 9. Proton Spectrum at $\theta_p = 30°$ from B^{10} Target Bombarded by 1.0 Mev Deuterons (used for energy calibration).

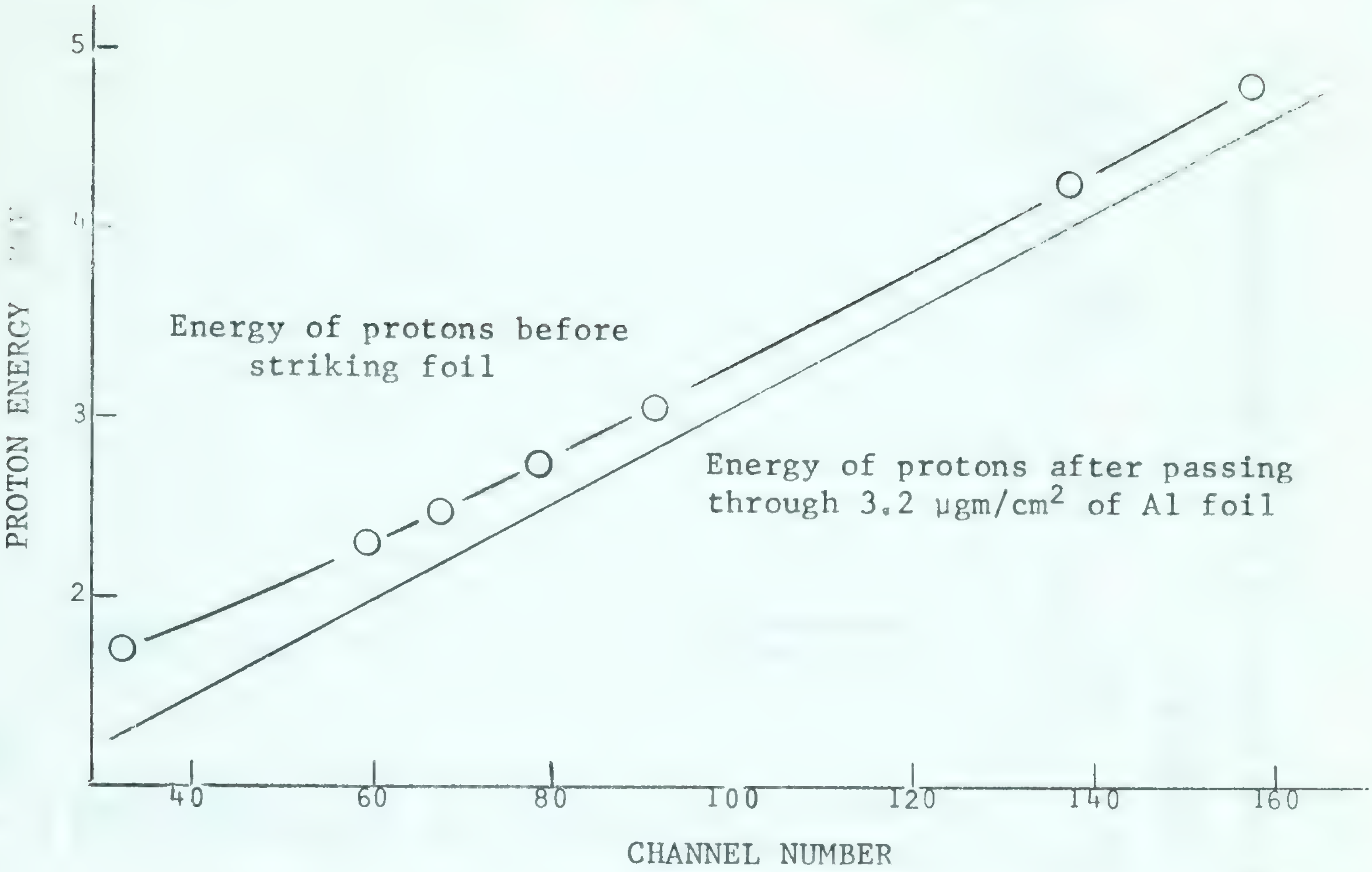

Figure 10. Energy Calibration Curve from Figure 9.

a considerable amount of carbon contamination on the O^{17} target (see C^{13} ground peak in Figure 11 and 12) it was deemed necessary to find the angular distribution of $C^{12}(d,p)C^{13}$ and $C^{13}(d,p)C^{14}$ in order that the C^{13} contamination might be subtracted from the O^{17} peak (see Figure 13 for proton spectrum from the natural carbon target).

The angular distribution of $C^{13}(d,p)C^{14}$ was measured at 1.0 Mev and 1.5 Mev on the C^{13} target and was compared with the angular distribution found using the natural carbon target. The agreement between the two angular distributions was within statistical error thus assuring that the peak from the natural carbon target was actually from $C^{13}(d,p)C^{14}$ ground. The angular distribution of $C^{12}(d,p)C^{13}$ was obtained from the natural carbon and the O^{17} target. The ratio of the number of counts at each angle measured in the $C^{12}(d,p)C^{13}$ angular distribution from the natural carbon target to those

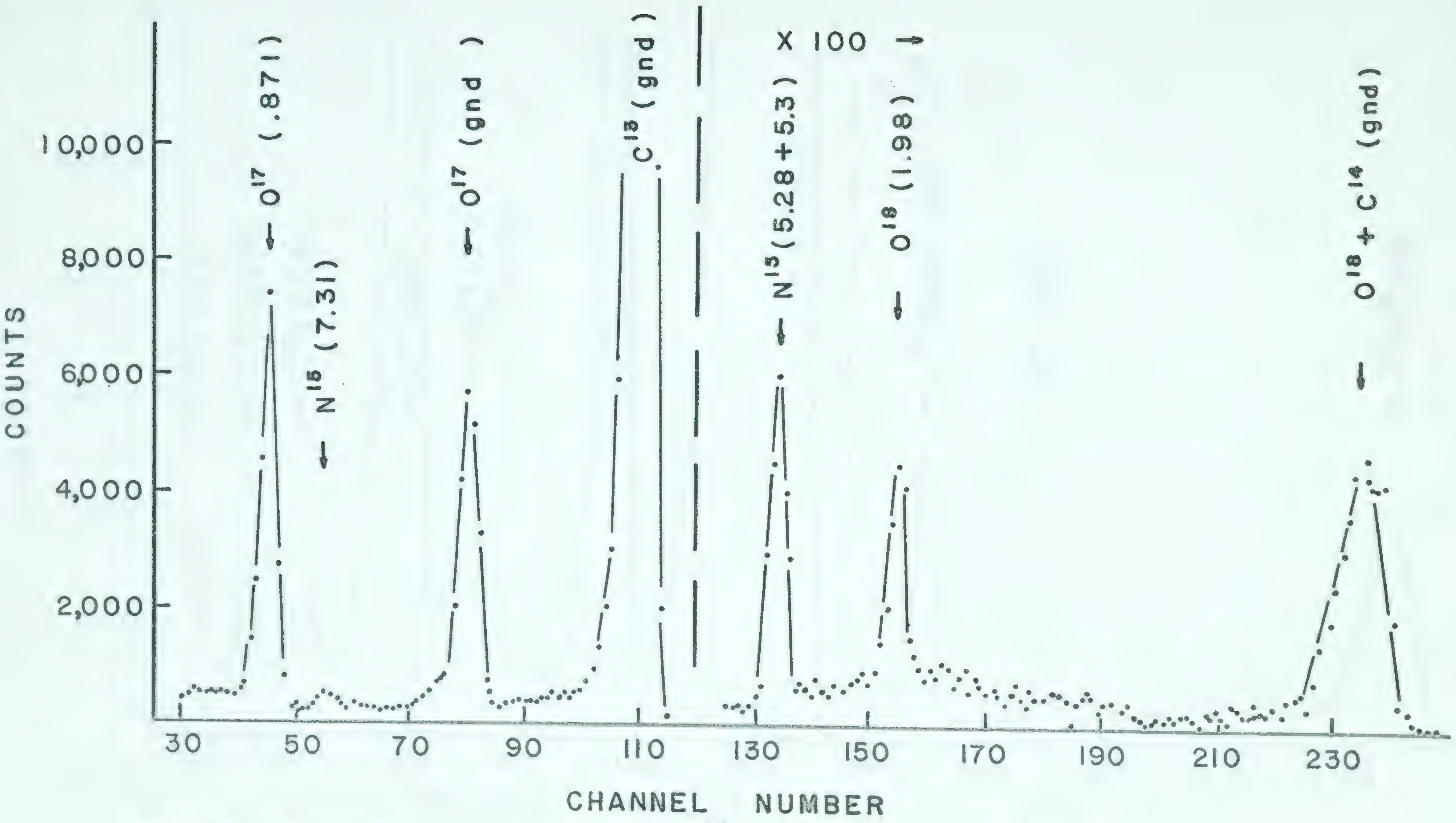

Figure 11. Proton Spectrum at θp = 30° from O^{17} Target Bombarded by 1.0 Mev Deuterons.

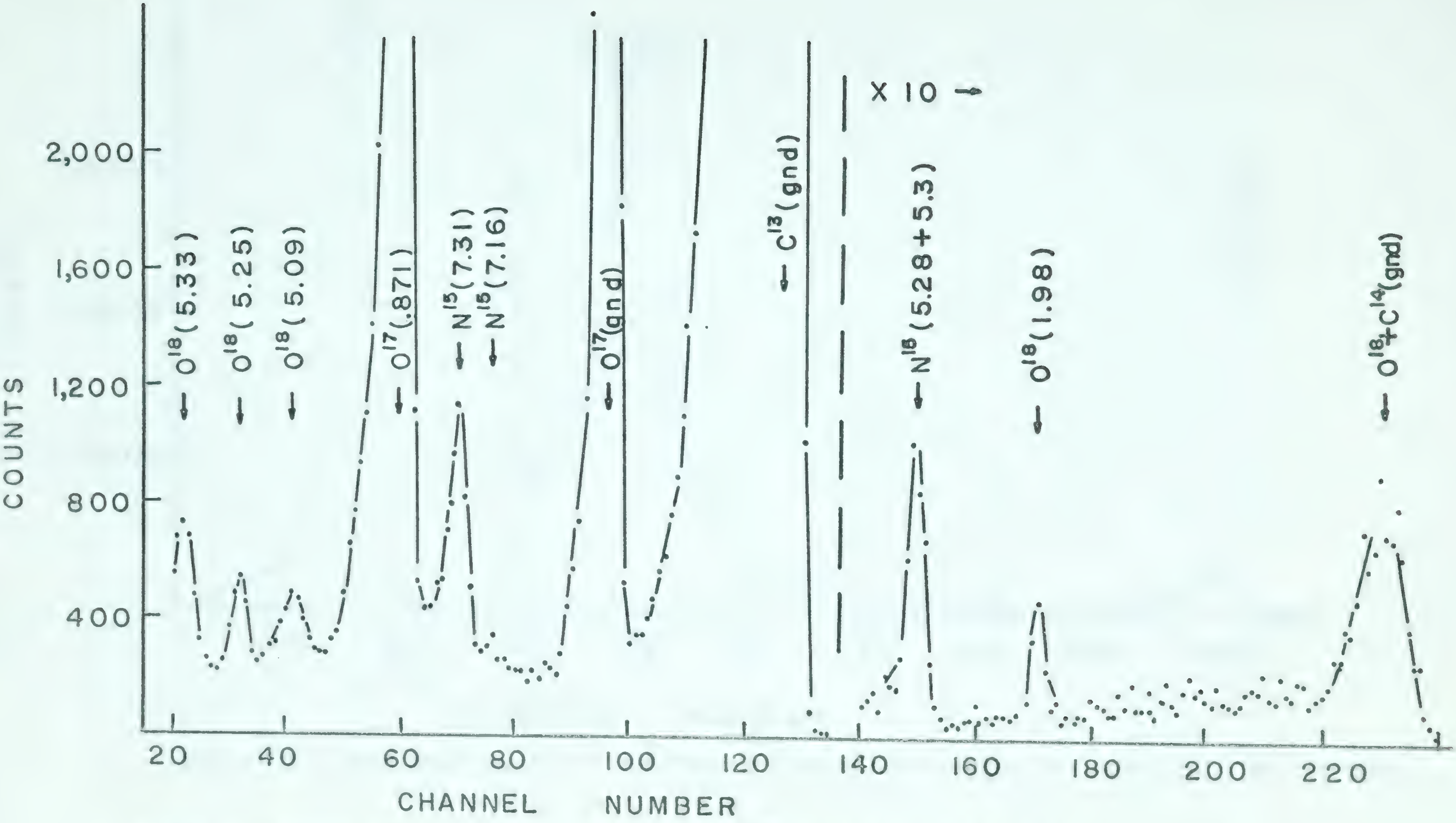

Figure 12. Proton Spectrum at θp = 30° from the O^{17} Target Bombarded by 1.5 Mev Deuterons.

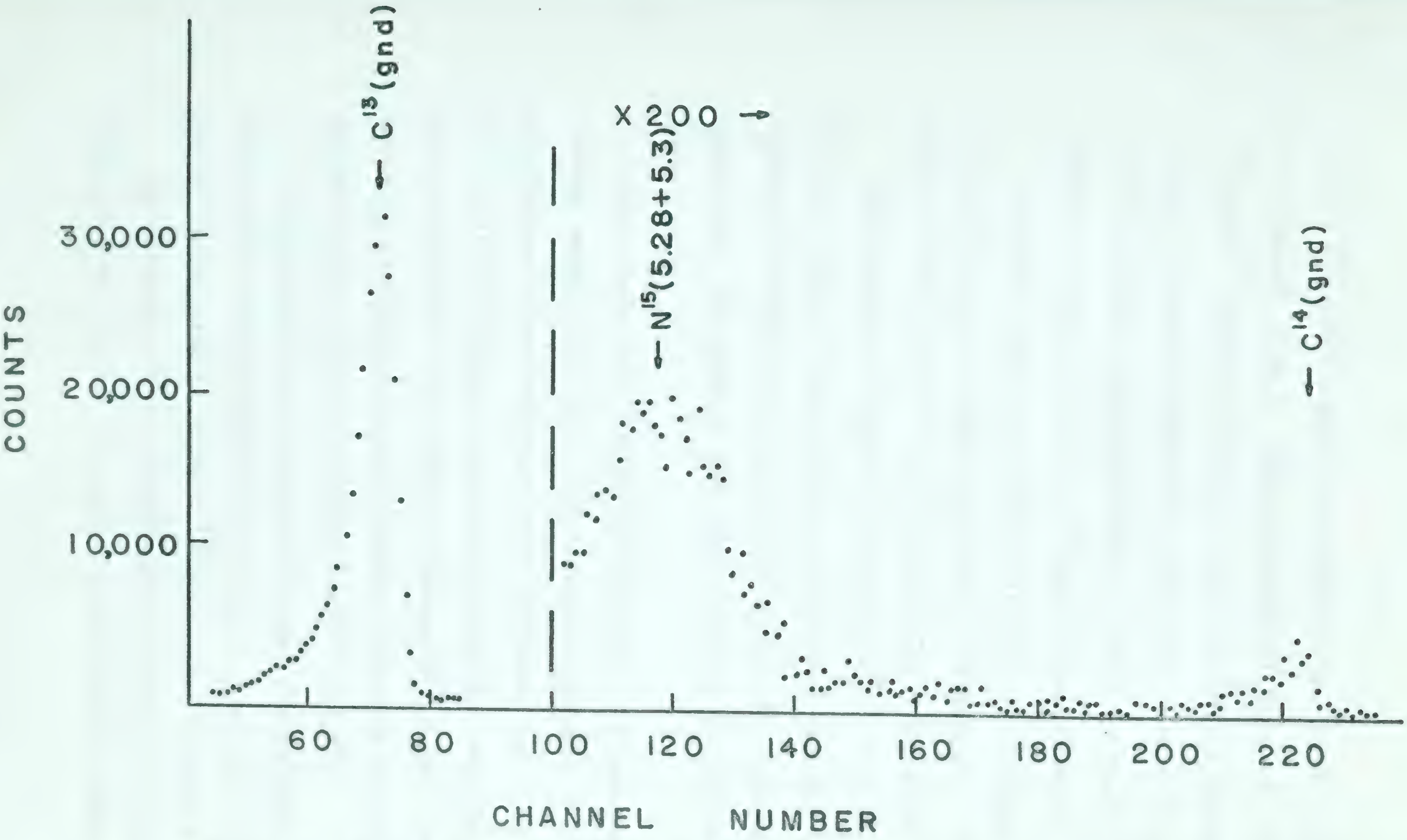

Figure 13. Proton Spectrum at θ_p = 30° from the Natural Carbon Target Bombarded by 1.5 Mev Deuterons.

in the $C^{12}(d,p)C^{13}$ angular distribution from the O^{17} target was found to be a constant (A_c/A_o). Thus the number of counts at each point in the $C^{13}(d,p)C^{14}$ angular distribution from the natural carbon target divided by A_c/A_o yielded the number of counts from $C^{13}(d,p)C^{14}$ on the O^{17} target. This allowed the contribution from C^{13} to be subtracted from the peak observed as being the sum of $C^{13}(d,p)C^{14}$(ground) and $O^{17}(d,p)^{18}$(ground).

Since the number of protons emitted in the formation of O^{18}(ground) was small as was the number from the C^{13} contaminant, the statistical error of the $O^{17}(d,p)O^{18}$ angular distribution was quite large.

The reaction $O^{16}(d,p)O^{17}$(ground) and O^{17*}(.871) was studied at 1.0 Mev and 1.5 Mev. There was little difficulty involved in obtaining the angular distributions because of the relatively high cross section (see Figure 14). The width of the peaks is due to the thickness of the SiO_2 target.

The results for $O^{16}(d,n)F^{17}$(ground and .500) were obtained at a bombarding energy of 3.5 Mev. The relative efficiency of the neutron detector (see Figure 15) was calculated by W. K. Dawson and G. C. Neilson by using the results of Goldberg, Anderson, Stoering and Wong (Go 61) with the reaction $T(p,n)He^3$ at a bombarding energy of 3.4 Mev. This was done for rough calibration purposes and was considered adequate for roughly determining the angular distribution of $O^{16}(d,n)F^{17}$.

The background rate for the $O^{16}(d,n)F^{17}$(ground and F^{17*}(.500) was estimated by visual inspection of the total spectrum at each angle from the Be^9 target as well as the Si^{30} target (see Figures 16 and 17).

The thickness of the natural carbon target was measured simply by weighing the carbon. The target holder plus the carbon was weighed

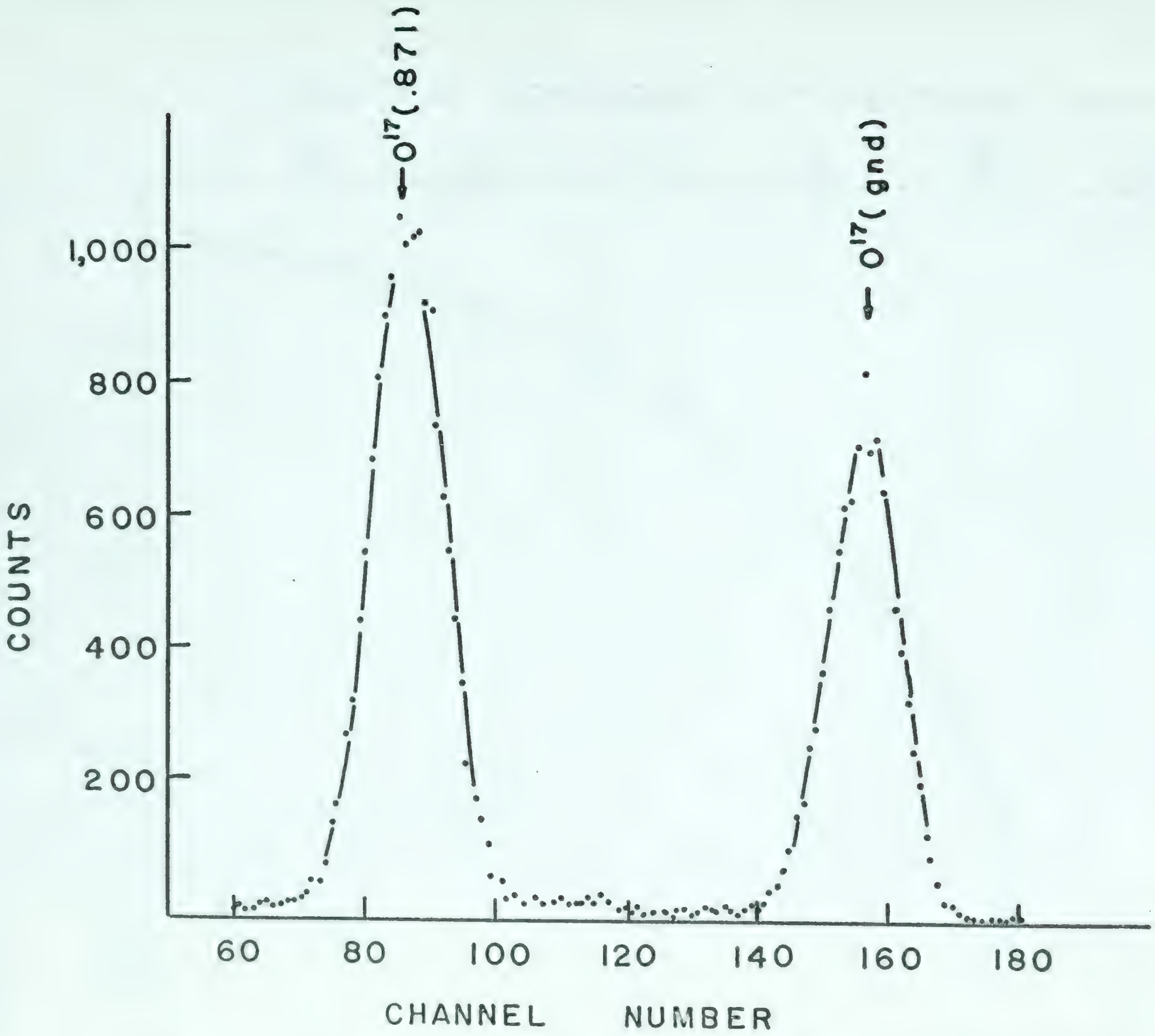

Figure 14. Proton Spectrum at θp = 30° from the SiO_2 Target Bombarded by 1.5 Mev Deuterons.

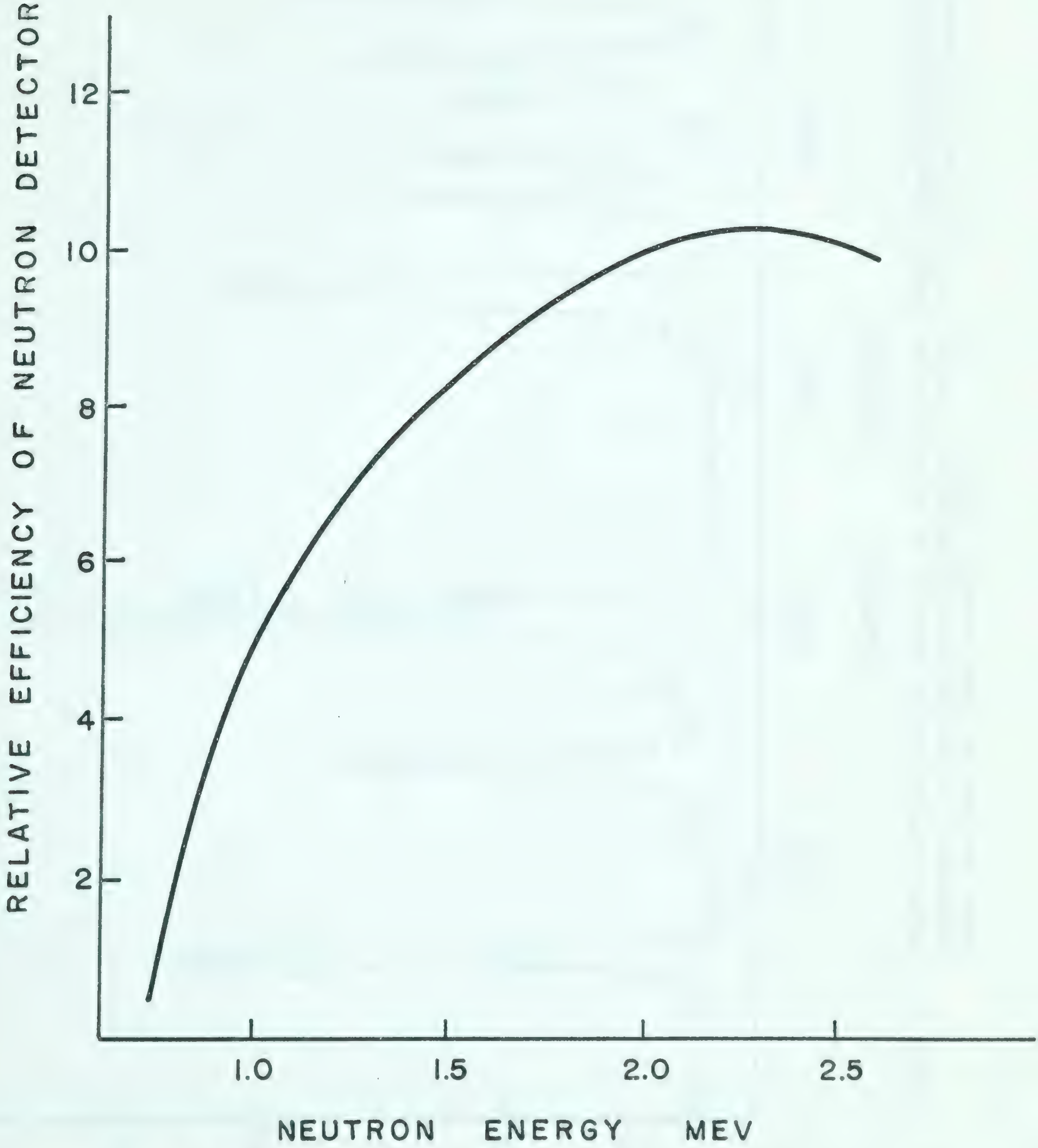

Figure 15. The Relative Efficiency of the Neutron Detector as Obtained Experimentally from the Reaction $T(p,n)He^3$ (Go 61).

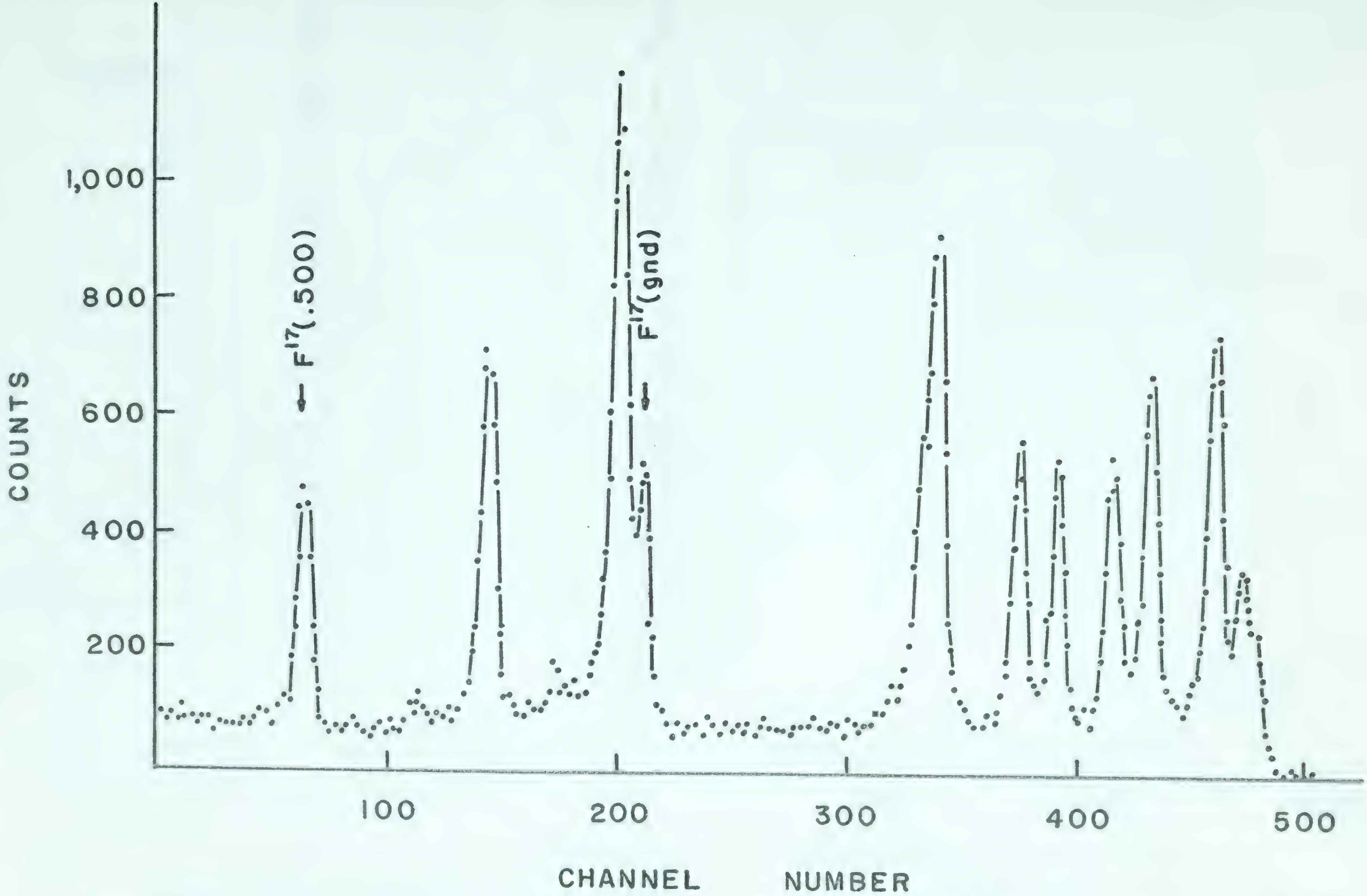

Figure 16. Neutron Time of Flight Spectrum at $\theta_N = 30°$ from the Be^9 Target Bombarded with 3.5 Mev Deuterons. The two peaks of interest are labelled $F^{17}(.500)$ and F^{17}(ground) and other peaks are from the reaction $Be^9(d,n)B^{10}$.

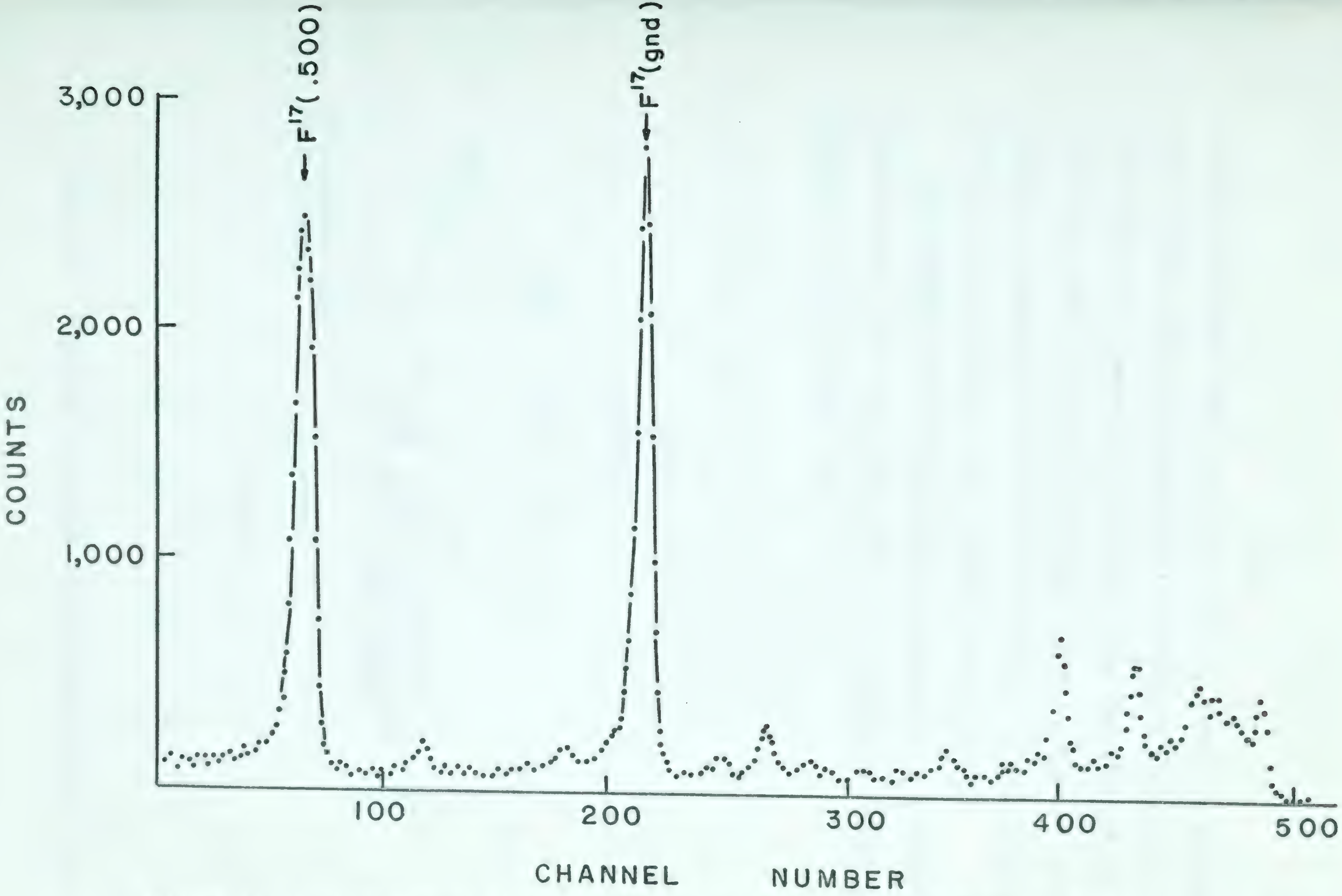

Figure 17. Neutron Time of Flight Spectrum at $\theta_N = 30°$ from the Si^{30} Target Bombarded with 3.5 Mev Deuterons. The two strong peaks are from $O^{16}(d,n)F17$(ground and .500). The other peaks are from the reaction $Si^{30}(d,n)P31$.

and then the target holder itself was weighed. There was an intermediate step in which half of the carbon was removed before weighing the backing for the purpose of making a rough check on the uniformity of the target. It was found that each half of the target weighed the same. This, of course, was insufficient evidence for uniformity but was at least consistent with that expected from a uniform layer of carbon.

The thickness of the SiO_2 target was measured with a Michelson Interferometer. The SiO_2 target, which is transparent, was placed in position as shown in Figure 18.

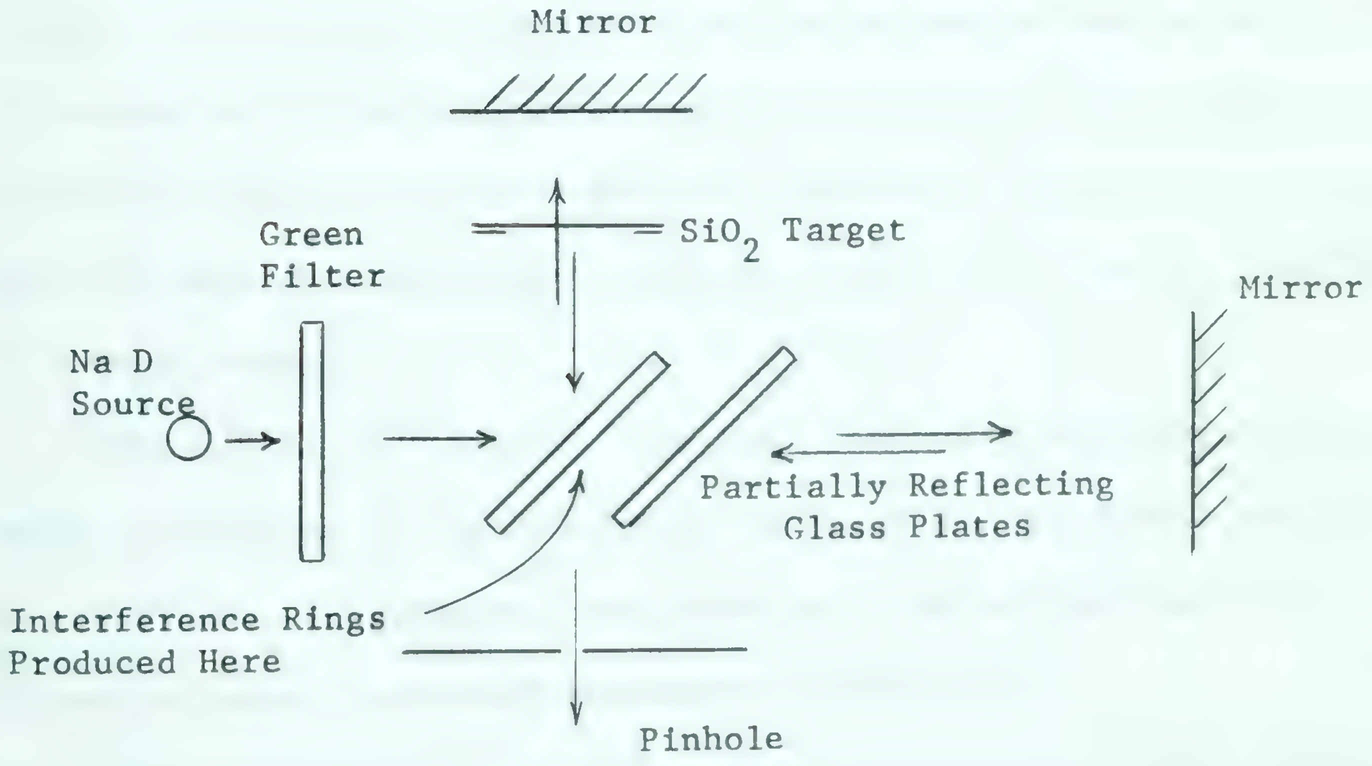

Figure 18. Michelson Interferometer for Measuring SiO_2 Target Thickness

The target was rotated by a known amount and the number of wave length shifts were counted. This procedure was repeated for different locations on the target to check for uniformity. With the data obtained from the Michelson Interferometer, the target thickness was calculated (see Appendix).

The solid angle of the effective area of the detector with respect to the beam spot on the target was measured for each target used. Thus, with the additional knowledge of target thicknesses and beam currents, the absolute cross sections were calculated.

The results obtained for $C^{12}(d,p)C^{13}$ at bombarding energies of 1.0 and 1.5 Mev are shown in Figure 19. The error in the relative height of points in the angular distribution was estimated to be about 5% because of the normalization to target current. The absolute cross section is estimated to have errors of about 20%. Most of these arose from the method of measuring target thickness, which was 330 $\mu gm/cm^2$ of natural carbon.

The reaction $C^{12}(d,p)C^{13}$ has been studied extensively in the range of energies 0.8 to 2.0 Mev by Kashy, Perry and Risser (Ka 59). The absolute cross sections were obtained by normalization to the Rutherford cross section of deuterons scattered by C^{12}.

The differential stripping cross section in the energy range 0.8 to 2.0 Mev exhibited several strong resonances corresponding to compound nucleus formation of levels in N^{14}. The angular distribution and absolute cross section was also determined by Kashy et al at deuteron energies of 0.92, 1.19, 1.31, 1.62 and 1.76 Mev.

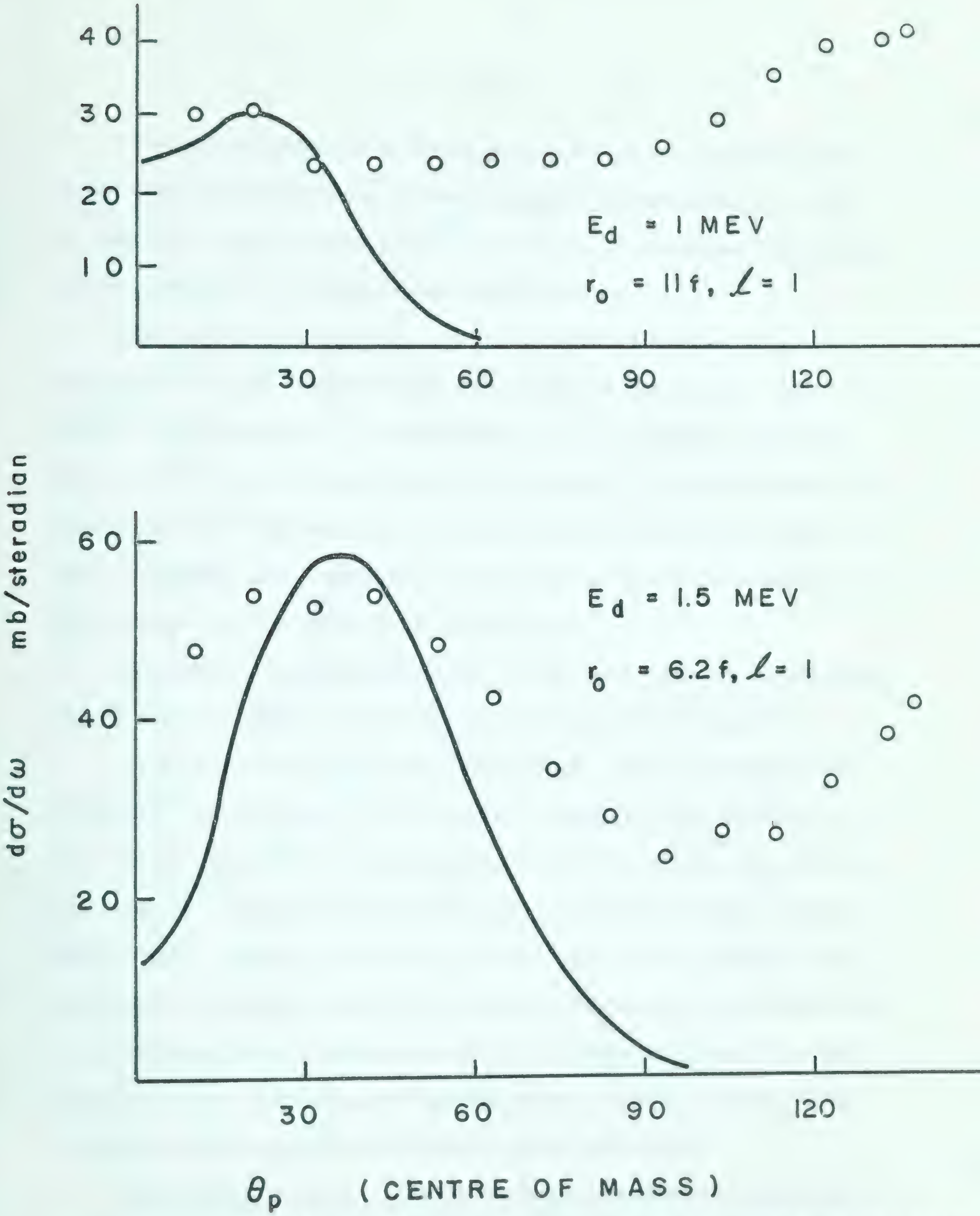

Figure 19. $C^{12}(d,p)C^{13}$ Angular Distribution of Protons Leading to the Ground State of C^{13}. The smooth curves are the predictions of Butler stripping theory.

The results obtained at bombarding energies of 1.0 and 1.5 Mev agree quite well with those of Kashy et al. The extremely poor fit of Butler stripping theory to $C^{12}(d,p)C^{13}$ can be accounted for because of the presence of a compound nucleus formation.

The angular distribution and absolute cross section of the reaction $C^{13}(d,p)C^{14}$(ground) were obtained from the natural carbon target (see Figure 20). The abundance of C^{12} is 98.892 so that the amount of C^{13} on the target was only 3.7 μgm/cm^2. Thus the number of counts in the C^{14}(ground) peak was quite small compared with those in the C^{13}(ground) peak. However, fairly good results were obtained as can be seen from the error bars in Figure 20.

In addition to the statistical errors there is a 20% uncertainty in the absolute cross section, as was the case for $C^{12}(d,p)C^{13}$.

V. K. Deshpande (De 63) has studied the reaction mechanism of $C^{13}(d,n)N^{14}$ and $C^{13}(d,p)C^{14}$ at energies between 3.2 and 4.1 Mev. In this energy range Butler stripping curves fit the angular distribution of $C^{13}(d,p)C^{14}$ quite well. This is not the case for energies of 1.0 and 1.5 Mev. However, the coulomb barrier for carbon is about 3 Mev and Butler stripping theory is not expected to be valid for bombarding energies below this. The broadening of the peaks in Figure 20 could possibly be due to the coulomb barrier alone, although further study is required before any such statement can be validated.

The absolute cross section at the peak calculated by Deshpande was about 4 millibarns per steradian and the cross section at 1.0 and

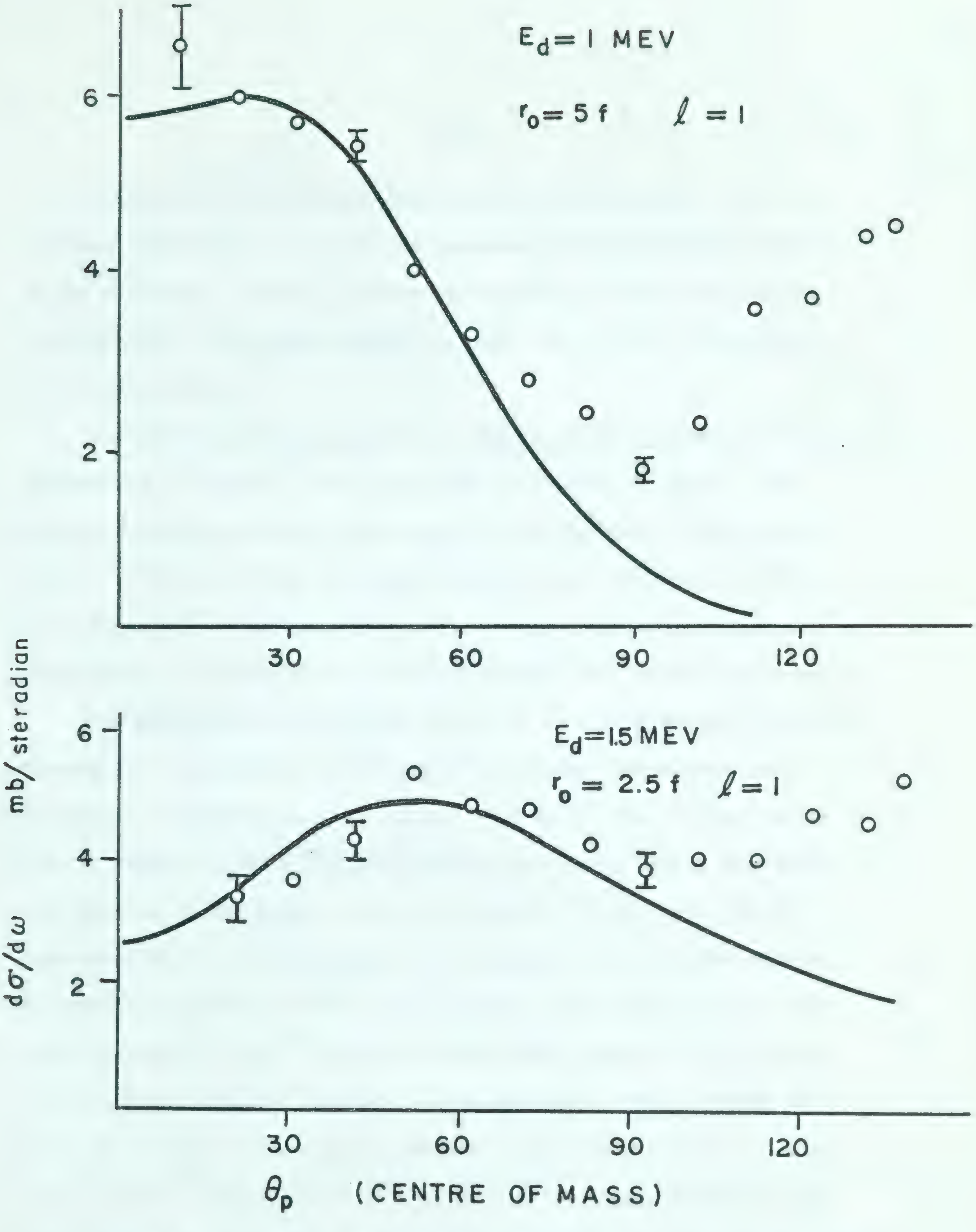

Figure 20. $C^{13}(d,p)C^{14}$ Angular Distribution of Protons Leading to Ground State of C^{13}. The smooth curves are the theoretical fits from Butler stripping theory.

1.5 Mev was 6 and 5 millibarns per steradian respectively. This may indicate that there is very little compound nucleus formation involved in the reaction. However, further measurements of the differential cross section in the energy range between 1 and 3.2 Mev are required to determine this.

The absolute cross sections and angular distributions of $O^{16}(d,p)O^{17}$ (ground) and $O^{16}(d,p)O^{17}(.871)$ are shown in Figures 21 and 22. The angular distributions were normalized to the .871 Mev γ rays emitted from $O^{17*}(.871)$ and then an average current was determined. A check at each angle by comparison with .871 Mev rays showed less than 5% fluctuation in effects of the target thickness and current measurement.

The method of normalization gave rise to a very smooth curve for the angular distribution of $O^{16}(d,p)O^{17}(.871)$ but introduced errors in the angular distribution of $O^{16}(d,p)O^{17}$(ground). The fluctuations seen in Figure 21 for $O^{16}(d,p)O^{17}$(ground) are quite likely due to the slowing down of deuterons in the SiO_2 target. It has been (Gr 56) determined by J. C. Grosskreutz that resonances occur in the differential cross sections of $O^{16}(d,p)O^{17}$(ground) and (.871) and that the cross section $O^{16}(d,p)O^{17}(.871)$ is rising more rapidly at 1.0 Mev and 1.5 Mev than $O^{16}(d,p)O^{17}$(ground). Thus the (d,p) cross section for deuterons slowed in the target would be reduced by a different amount for $O^{16}(d,p)O^{17}$(ground) than $O^{16}(d,p)O^{17}(.871)$. The thickness of the SiO_2 target was 546 μgms/cm^2 within 10% error and thus the absolute cross section is about 15% in error.

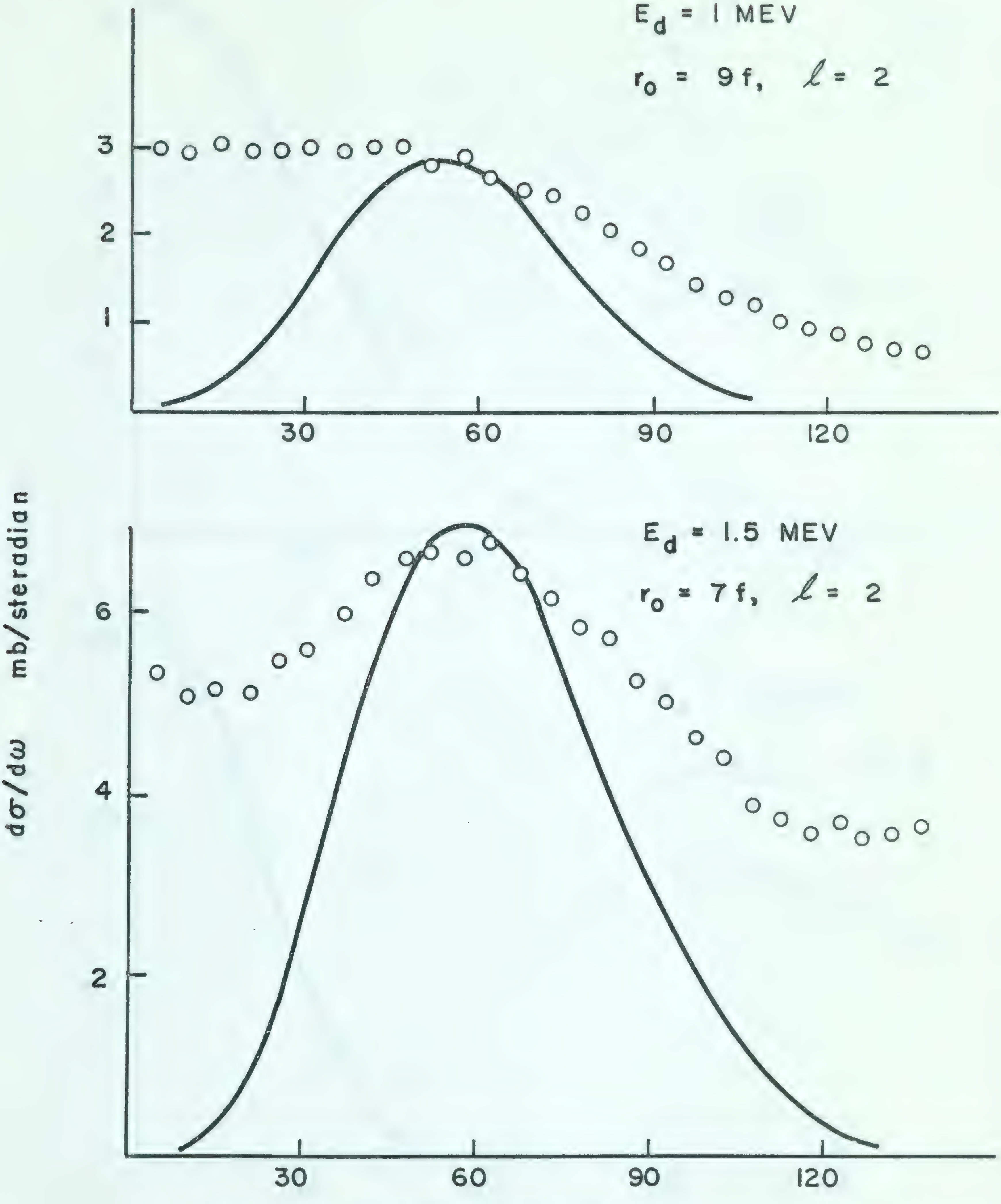

Figure 21. $O^{16}(d,p)O^{17}$ Angular Distribution of Protons Leading to the Ground State of O^{17}. The smooth curves are the predictions of Butler stripping theory.

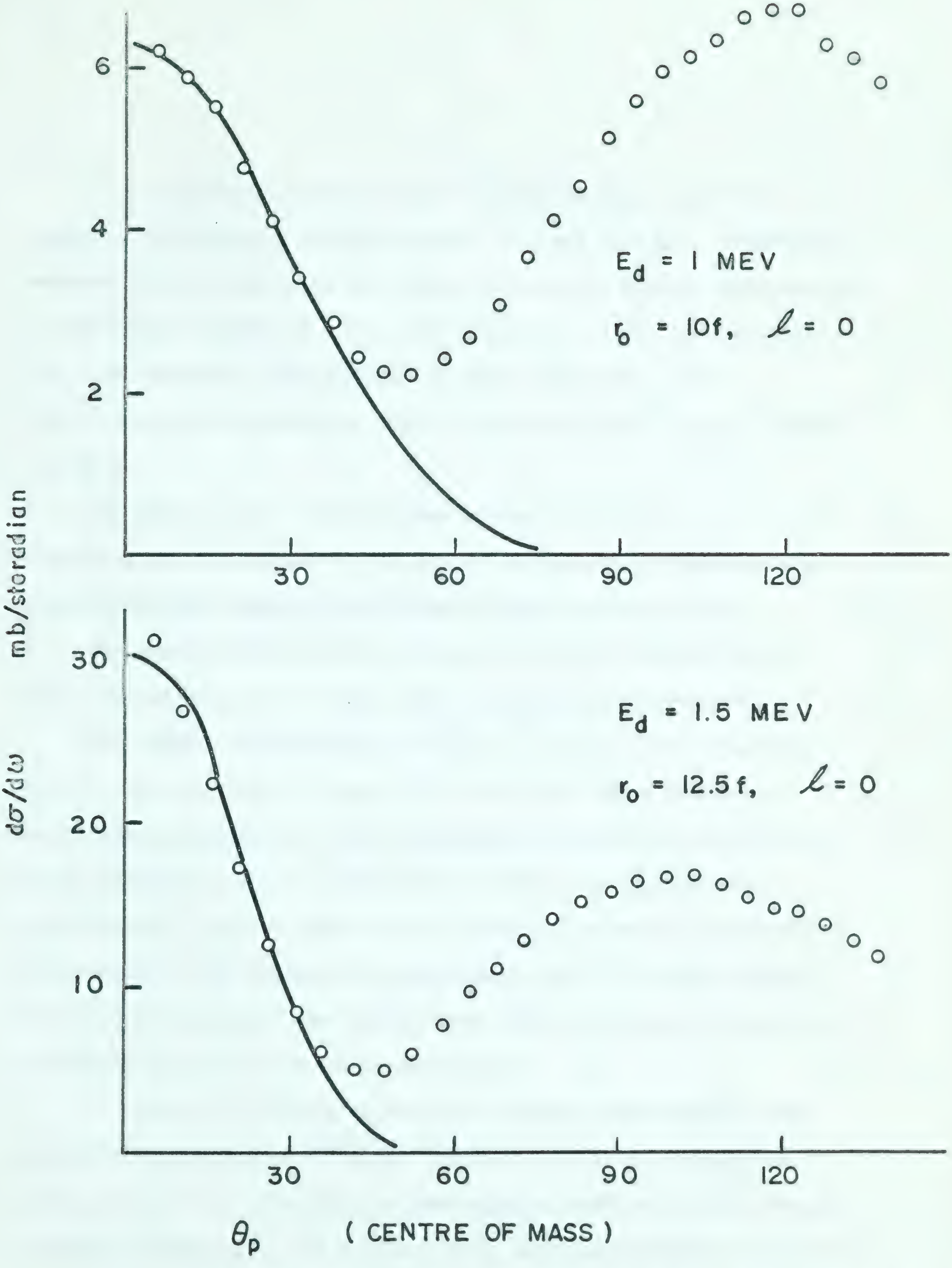

Figure 22. $O^{16}(d,p)O^{17}$ Angular Distribution of Protons Leading to the First Excited State of O^{17}. The smooth curves are the fits from Butler stripping theory.

[illegible]

J. C. Grosskreutz studied the $O^{16}(d,p)O^{17}$(ground and .871) reactions at bombarding energies between 1.05 and 2.51 Mev. Grosskreutz measured the absolute cross sections as well as the angular distributions at bombarding energies of 1.05, 1.35, 1.60, 1.76, 2.01, 2.26 and 2.51 Mev. Two resonances were observed in this energy range, one at about 1.6 Mev and the other at about 2.4 Mev for both $O^{16}(d,p)O^{17}$(ground and .871).

The existence of the resonances in the differential cross section along with the flat shapes of the angular distributions indicates that compound nucleus formation contributes strongly to the reaction.

The angular distributions and absolute cross sections shown in Figure 21 and 22 agree very well with the results of Grosskreutz.

The angular distributions of $O^{16}(d,n)F^{17}$(ground and .5 Mev) with E_d = 3.5 Mev are shown in Figure 23. Most of the error involved is in estimating background, which introduces an estimated 5% uncertainty. Butler theory fits the F^{17} ground state angular distribution only approximately. In this case with the negative Q value the theoretical curve is quite flat whereas the experimental curve is strongly peaked, thus demonstrating that the Butler theory does not necessarily apply at bombarding energies above the coulomb barrier.

B. Yaramis (Ya 61) has measured the absolute cross sections and angular distributions of $O^{16}(d,n)F^{17}$(ground and 0.5) at a bombarding energy of 5.02 Mev. The shapes of the angular distribution were similar to those in Figure 23. The absolute cross sections determined by Yaramis

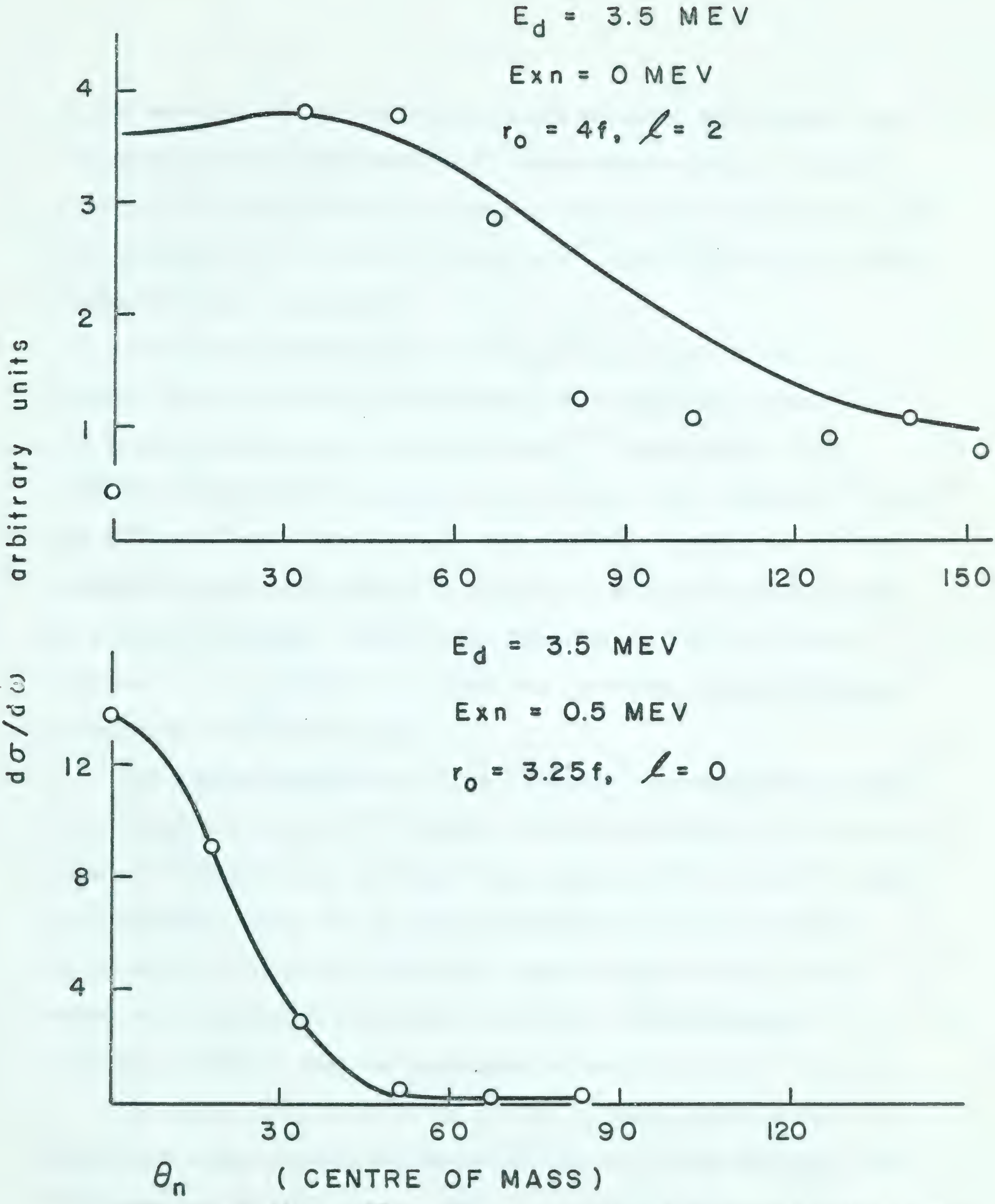

Figure 23. $O^{16}(d,n)F^{17}$ Angular Distribution of Neutrons Leading to the Ground and First Excited State of F^{17}. The smooth curves are the theoretical fits from Butler stripping theory.

at the peaks were 27 and 138 millibarns per steradian for neutrons from the ground state and .500 state of F^{17} respectively with $E_d = 5.02$ Mev. A good fit of Butler theory to the angular distribution of $O^{16}(d,n)F^{17}(.5)$ was found with $r_o = 4.0$ fermi. The fit to $O^{16}(d,n)F^{17}$(ground) was similar to the fit shown in Figure 23.

The angular distribution of $O^{17}(d,p)O^{18}$ was very difficult to obtain. It was found that the absolute cross section was extremely low and to make matters worse there was enough C^{13} contamination on the target to account for the majority of the counts in the combined $O^{17}(d,p)O^{18}$ and $C^{13}(d,p)C^{14}$ peak. The delicate 25 μ inch foil in which the O^{17} was imbedded was mounted on another 20 μ inch foil which was already mounted on a heavy Ni backing. Thus C^{13} was present on the back and front of each foil. Any structure in the peak was, therefore, almost meaningless in defining the O^{18}(ground) peak.

The angular distribution of the $C^{12}(d,p)C^{13}$ reaction was extracted from the spectra from the O^{17} target. From the knowledge of the absolute cross of $C^{12}(d,p)C^{13}$ and $C^{13}(d,p)C^{14}$ the amount of C^{13} on the O^{17} target was determined. After all of these calculations were done the result was as shown in Figure 24. The points shown in Figure 24 have large errors which arise from statistical error only. The main source of statistical error is from the uncertainty of the amount of C^{13} present.

The reason that no points are plotted at large angles is that the statistical error involved was almost 100% because of the low count rate. There were indications, however, that if a backward maximum exists, it is much smaller than the forward maximum.

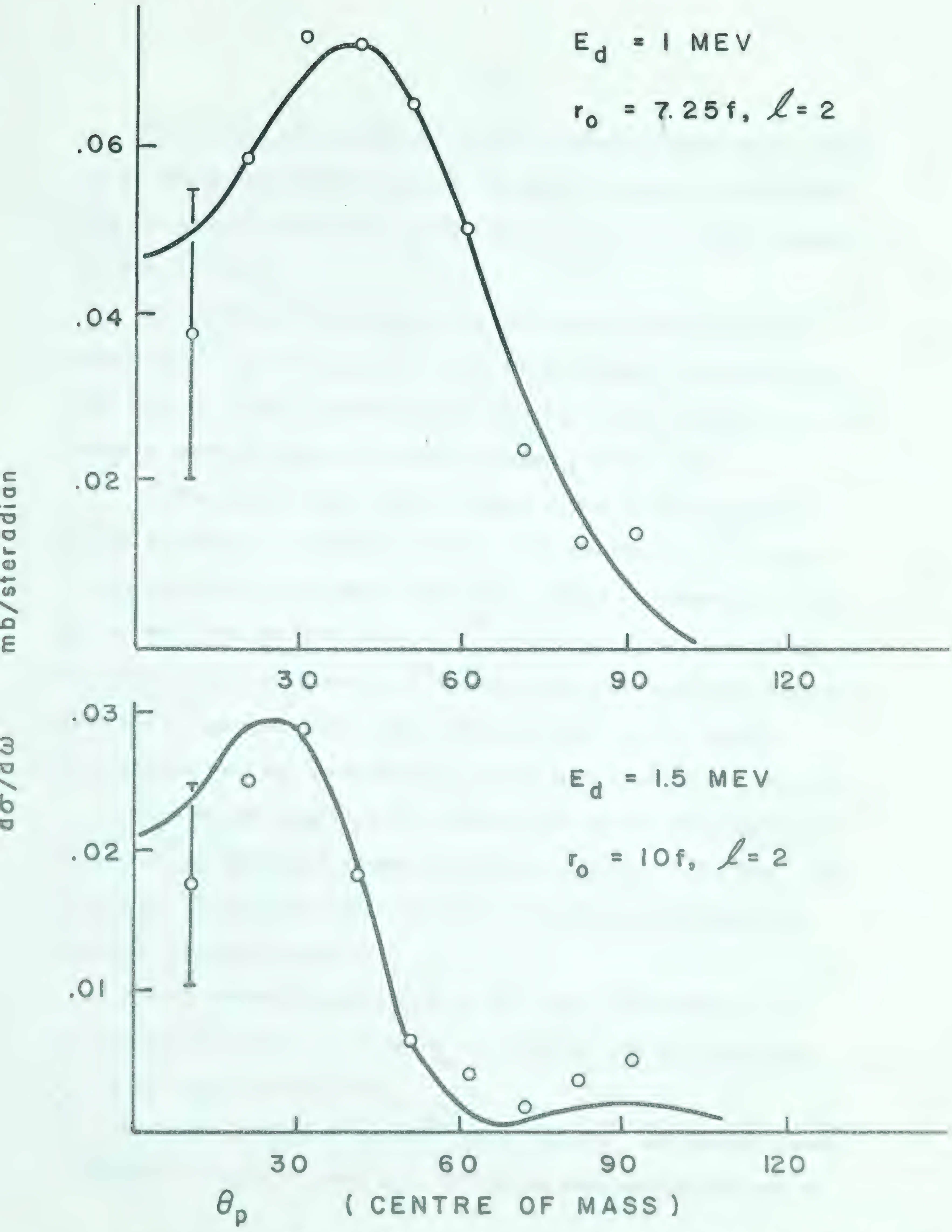

Figure 24. $O^{17}(d,p)O^{18}$ Angular Distributions of Protons Leading to the Ground State of O^{18}. The smooth curves are the theoretical fits from Butler stripping theory.

It is quite surprising that Butler stripping theory gives a good fit to the angular distribution at 1.0 and 1.5 Mev when one considers that the errors involved are quite large and that the coulomb barrier is about 3.8 Mev.

The absolute cross section was calculated assuming that the amount of O^{17} was 111 μgm/cm^2. It is quite unlikely that there were more than 111 μgm/cm^2 present on the target, so that the absolute cross sections shown in Figure 24 should indicate a lower limit.

Ahnlund (Ah 54) bombarded an oxygen target of 1% enrichment of O^{17} at an energy of 0.855 Mev with $\theta_p = 61°$ and 134.7°. The oxygen was collected on a 0.28 mg/cm^2 gold foil. Peaks corresponding to the ground and first excited state of O^{18} were observed to be very weak. The peak corresponding to the C^{14}(ground) state was much more prominent than the O^{18}(ground) state peak. The resolution of the magnetic spectrometer used was good enough to allow separation of the two peaks.

Bilaniuk and Hough (Bi 57) obtained the angular distribution of $O^{17}(d,p)O^{18}$(ground) and 1.99 and 3.55 levels with $E_d = 7.772$ Mev. They also found the absolute cross section to be very small although no numerical estimate was made.

Butler curves gave good fits to all three levels with $\ell_n = 2$ for the ground state, $\ell_n = 0$ and $\ell_n = 2$ for the 1.99 Mev level and $\ell_n = 2$ for the 3.55 Mev level.

Deshpande studied $C^{13}(d,n)N^{14}$ and $C^{13}(d,p)C^{14}$ and (De 63) found a secondary maximum at about $\theta_n = 80°$ in the angular distribution of

$C^{13}(d,n)N^{14}$. This peak does not occur in the $C^{13}(d,p)C^{14}$ angular distribution and is thought to correspond to the $\ell_n = 3$ peak allowed by exchange stripping, the primary peak in each case being $\ell_n = 1$.

There is a great deal of similarity between C^{13} and O^{17} in that the last neutron in each case is probably in a single particle state moving around the more stable configuration of 6n and 6p in one case and 8n and 8p in the other. This is what prompted the study of the reaction mechanism of $O^{17}(d,n)F^{18}$ and $O^{17}(d,p)O^{18}$.

It has been determined that the absolute cross section of $O^{17}(d,p)O^{18}$ is extremely small. Thus it would be expected that the absolute cross section $O^{17}(d,n)F^{18}$ would also be small. This will, of course, hinder experimentalists from gaining knowledge about the reaction mechanisms involved in $O^{17}(d,n)F^{18}$. Any detailed study of the angular distribution $O^{17}(d,n)F^{18}$(ground) and $O^{17}(d,p)O^{18}$(ground) would be very time consuming. However, if there is an appreciable amount of exchange stripping involved in the $O^{17}(d,n)F^{18}$ reaction, another peak would appear in the angular distribution corresponding to $\ell = 4$. The angular distribution obtained from $O^{17}(d,p)O^{18}$(ground) indicates that the reaction is direct and thus comparison of $O^{17}(d,n)F^{18}$ and $O^{17}(d,p)O^{18}$ would be simplified.

Butler theory has not been successful in predicting absolute cross sections. However, it is of interest to determine the ratio of absolute cross sections of two closely related levels.

The ratio of two cross sections is (Lu 57):

$$\frac{\frac{d\sigma_1}{d\omega}}{\frac{d\sigma_2}{d\omega}} = \frac{r^2_{o_1}\ (2J_{f_1}+1)(2J_{o_2}+1)\ \sqrt{E_{f_1}}\ |f_{o_1}|^2\ \delta^{\ell}_{TAB_1}}{r^2_{o_2}\ (2J_{o_1}+1)(2J_{f_2}+1)\ \sqrt{E_{f_2}}\ |f_{o_2}|^2\ \delta^{\ell}_{TAB_2}}$$

$|f|^2$ can be obtained from Lubitz tables for single particle states only. $|f|^2$ would not be expected to affect the value of the ratio of two cross sections by more than a factor of about four. The ratios of absolute cross sections (neglecting $|f|^2$) are shown in the Table below.

REACTION	E_d(Mev)	RATIO AT PEAK (Butler)	RATIO AT PEAK (Experimental)
$\frac{O^{16}(d,p)O^{17}}{O^{17}(d,p)O^{18}}$	1.0	27	40 (or less)
$\frac{O^{16}(d,p)O^{17}}{O^{17}(d,p)O^{18}}$	1.5	105	240 (or less)
$\frac{C^{12}(d,p)C^{13}}{C^{13}(d,p)C^{14}}$	1.0	3	9
$\frac{C^{12}(d,p)C^{13}}{C^{13}(d,p)C^{14}}$	1.5	3	8

The experimental ratio is larger in all four cases than the theoretical ratio and this is possibly due to the compound nucleus formation in $C^{12}(d,p)C^{13}$ and $O^{16}(d,p)O^{17}$ which is not accounted for by Butler theory. There is evidence of very little compound nucleus formation in the $C^{13}(d,p)C^{14}$ reaction and it is unlikely that compound nucleus formation contributes much to the $O^{17}(d,p)O^{18}$ cross section since Butler theory fits the angular distributions well.

BIBLIOGRAPHY

Ah 54. Katarina Ahnlund, Phys. Rev. 96, 999-1000, 1954.

Ba 56. D. R. Bach and P. V. C. Hough, Phys. Rev. 102, 1341-1344, 1956.

Bi 57. O. M. Bilaniuk and P. V. C. Hough, Phys. Rev. 108, 305-310, 1957.

Bu 51. S. T. Butler, Proc. Roy. Soc. (London) 208A, 559, 1951.

Bu 57. S. T. Butler, Nuclear Stripping Reactions, John Wiley & Sons Inc., New York, 1957.

De 63. V. K. Despande, Nuclear Physics 47, 257-65, 1963.

Go 61. M. D. Goldberg, J. D. Anderson, J. P. Stoering, and C. Wong, Phys. Rev. 122, 1510, 1961.

Gr 56. J. C. Grosskreutz, Phys. Rev. 101, 706-709, 1956.

Ka 59. E. Kashy, R. R. Perry, and J. R. Risser, Phys. Rev. 117, 1289-1296, 1959.

Lu 57. C. R. Lubitz, Numerical Tables of Butler-Born Approximation Stripping Cross Sections, University of Michigan, 1957.

Mo 52. R. C. Mobley, Phys. Rev. 88, 360-361, 1952.

Ol 64. W. C. Olsen, Ph.D. Thesis, University of Alberta, 1964.

Ri 54. M. Rich and R. Mady, UCRL-2301, 1954.

Wh 58. Ward Whaling, Handbuch der Physik 34, 193, 1958.

Ya 61. B. Yaramis, Phys. Rev. 124, 836-838, 1961.

APPENDIX

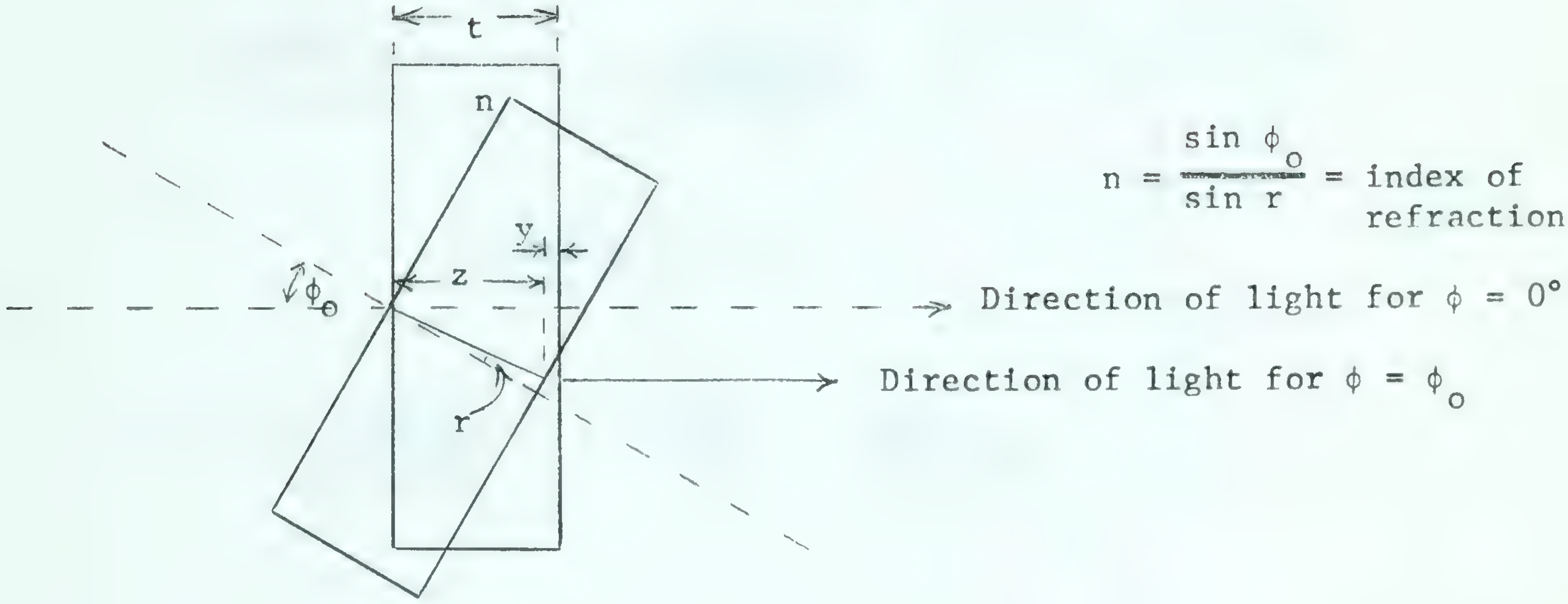

$$n = \frac{\sin \phi_o}{\sin r} = \text{index of refraction}$$

$\cos r = t/x$

$\cos (\phi_o - r) = z/x$

$y = t - z$

$$z = x(\cos \phi_o \cos r + \sin \phi_o \sin r)$$

$$y = t - x(\cos \phi_o \sqrt{1 - \frac{\sin^2 \phi_o}{n^2}} + \sin \phi_o \frac{\sin \phi_o}{n}$$

$$y = t - x \frac{\cos \phi_o}{n} \sqrt{n^2 - \sin^2 \phi_o} + \frac{\sin^2 \phi_o}{n}$$

The optical path through the quartz = nx.

$$x = \frac{t}{\cos r} = \frac{nt}{\sqrt{n^2 - \sin^2 \phi_o}}$$

At $\phi = \phi_o$ the optical path = $nx + y$

At $\phi = 0$ the optical path = nt

Therefore, the change in the optical path

$$\Delta = nx + y - nt$$

$$= \frac{n^2 t}{n - \sin^2\phi_o} + t - \frac{nt}{\sqrt{n^2-\sin^2\phi_o}} \left\{ \frac{\cos\phi_o \quad n^2-\sin^2\phi_o}{n} + \frac{\sin^2\phi}{n} \right\} - nt$$

$$\Delta = t \left\{ \frac{n^2}{\sqrt{n^2-\sin^2\phi_o}} + 1 - \frac{\cos\phi_o}{n} - \frac{\sin^2\phi}{\sqrt{n^2-\sin^2\phi_o}} - n \right\}$$

$$= t\ (\sqrt{n^2-\sin^2\phi_o} + 1 - \cos\phi_o - n)$$

Since the light traverses the quartz twice in the Michelson Interferometer,

$$t = \frac{\Delta}{\sqrt{n^2 - \sin^2\phi_o} + 1 - \cos\phi_o - n} = \frac{N/2\lambda}{\sqrt{n^2 - \sin^2\phi_o} + 1 - \cos\phi_o - n}$$

where N is the number of shifts for $\phi = 0$ to ϕ_o and $\lambda = 5893$ angstroms for Na D.

The formula for t with $\phi = \phi_1$ and $\phi = \phi_2$ where N_1 and N_2 are known is

$$t = \frac{(N_2 - N_1)\lambda}{2(\sqrt{n^2 - \sin^2\phi_2} - \sqrt{n^2 - \sin^2\phi_1} + \cos\phi_1 - \cos\phi_2)}$$